Canopy-scale biophysical controls of transpiration and evaporation in the Amazon Basin

Mallick, Kaniska; Trebs, Ivonne; Bøgh, Eva; Giustarini, Laura; Schlerf, Martin; Drewry, Darren T.; Hoffmann, Lucien; von Randow, Celso; Kruijt, Bart; Araùjo, Alessandro; Saleska, Scott; Ehleringer, James R.; Domingues, Tomas F.; Ometto, Jean Pierre H.B.; Nobre, Antonio D.; de Moraes, Osvaldo Luis Leal; Hayek, Matthew; Munger, J. William; Wofsy, Steven C.

Published in:
Hydrology and Earth System Sciences

DOI:
10.5194/hess-2015-552

Publication date:
2016

Document Version
Publisher's PDF, also known as Version of record

Citation for published version (APA):
Mallick, K., Trebs, I., Bøgh, E., Giustarini, L., Schlerf, M., Drewry, D. T., Hoffmann, L., von Randow, C., Kruijt, B., Araùjo, A., Saleska, S., Ehleringer, J. R., Domingues, T. F., Ometto, J. P. H. B., Nobre, A. D., de Moraes, O. L. L., Hayek, M., Munger, J. W., & Wofsy, S. C. (2016). Canopy-scale biophysical controls of transpiration and evaporation in the Amazon Basin. *Hydrology and Earth System Sciences*, *20*(10), 4237-4264. https://doi.org/10.5194/hess-2015-552

Hydrol. Earth Syst. Sci., 20, 4237–4264, 2016
www.hydrol-earth-syst-sci.net/20/4237/2016/
doi:10.5194/hess-20-4237-2016

Hydrology and Earth System Sciences
Open Access
EGU

Canopy-scale biophysical controls of transpiration and evaporation in the Amazon Basin

Kaniska Mallick[1], Ivonne Trebs[1], Eva Boegh[2], Laura Giustarini[1], Martin Schlerf[1], Darren T. Drewry[3,12], Lucien Hoffmann[1], Celso von Randow[4], Bart Kruijt[5], Alessandro Araùjo[6], Scott Saleska[7], James R. Ehleringer[8], Tomas F. Domingues[9], Jean Pierre H. B. Ometto[4], Antonio D. Nobre[4], Osvaldo Luiz Leal de Moraes[10], Matthew Hayek[11], J. William Munger[11], and Steven C. Wofsy[11]

[1]Department of Environmental Research and Innovation, Luxembourg Institute of Science and Technology (LIST), L4422, Belvaux, Luxembourg
[2]Department of Science and Environment, Roskilde University, Roskilde, Denmark
[3]Jet Propulsion Laboratory, California Institute of Technology, 4800 Oak Grove Drive, Pasadena, 91109, USA
[4]Instituto Nacional de Pesquisas Espaciais (INPE), Centro de Ciência do Sistema Terrestre, São José dos Campos, SP, Brazil
[5]Wageningen Environmental Research (ALTERRA), Wageningen, the Netherlands
[6]Empresa Brasileira de Pesquisa Agropecuária (EMBRAPA), Belém, PA, Brazil
[7]Department of Ecology and Evolutionary Biology, University of Arizona, Tucson, AZ, USA
[8]Department of Biology, University of Utah, Salt Lake City, UT, USA
[9]Faculdade de Filosofia Ciências e Letras de Ribeirão Preto, Universidade de São Paulo (USP), São Paulo, SP, Brazil
[10]Centro Nacional de Monitoramento e Alertas de Desastres Naturais, São Paulo, SP, Brazil
[11]Department of Earth and Planetary Science, Harvard University, Cambridge, MA, USA
[12]Joint Institute for Regional Earth System Science and Engineering, University of California, Los Angeles, California, USA

Correspondence to: Kaniska Mallick (kaniska.mallick@gmail.com) and Ivonne Trebs (ivonne.trebs@list.lu)

Received: 30 December 2015 – Published in Hydrol. Earth Syst. Sci. Discuss.: 27 January 2016
Revised: 21 June 2016 – Accepted: 14 September 2016 – Published: 19 October 2016

Abstract. Canopy and aerodynamic conductances (g_C and g_A) are two of the key land surface biophysical variables that control the land surface response of land surface schemes in climate models. Their representation is crucial for predicting transpiration (λE_T) and evaporation (λE_E) flux components of the terrestrial latent heat flux (λE), which has important implications for global climate change and water resource management. By physical integration of radiometric surface temperature (T_R) into an integrated framework of the Penman–Monteith and Shuttleworth–Wallace models, we present a novel approach to directly quantify the canopy-scale biophysical controls on λE_T and λE_E over multiple plant functional types (PFTs) in the Amazon Basin. Combining data from six LBA (Large-scale Biosphere-Atmosphere Experiment in Amazonia) eddy covariance tower sites and a T_R-driven physically based modeling approach, we identified the canopy-scale feedback-response mechanism between g_C, λE_T, and atmospheric vapor pressure deficit (D_A), without using any leaf-scale empirical parameterizations for the modeling. The T_R-based model shows minor biophysical control on λE_T during the wet (rainy) seasons where λE_T becomes predominantly radiation driven and net radiation (R_N) determines 75 to 80 % of the variances of λE_T. However, biophysical control on λE_T is dramatically increased during the dry seasons, and particularly the 2005 drought year, explaining 50 to 65 % of the variances of λE_T, and indicates λE_T to be substantially soil moisture driven during the rainfall deficit phase. Despite substantial differences in g_A between forests and pastures, very similar canopy–atmosphere "coupling" was found in these two biomes due to soil moisture-induced decrease in g_C in the pasture. This revealed the pragmatic aspect of the T_R-driven model behavior that exhibits a high sensitivity of g_C to per unit change in wetness as opposed to g_A that is marginally sensitive to surface wetness variability. Our results reveal the occurrence of a significant hysteresis between λE_T and g_C during the dry season for the

pasture sites, which is attributed to relatively low soil water availability as compared to the rainforests, likely due to differences in rooting depth between the two systems. Evaporation was significantly influenced by g_A for all the PFTs and across all wetness conditions. Our analytical framework logically captures the responses of g_C and g_A to changes in atmospheric radiation, D_A, and surface radiometric temperature, and thus appears to be promising for the improvement of existing land–surface–atmosphere exchange parameterizations across a range of spatial scales.

1 Introduction

The Amazon rainforest is one of the world's most extensive natural ecosystems, influencing the Earth's water, energy, and carbon cycles (Malhi, 2012), and is also a major source of global terrestrial evapotranspiration (E) or latent heat flux (λE) (Costa et al., 2010; Harper et al., 2014). An intensification of the Amazon hydrological cycle was observed in the past 2 decades (Cox et al., 2000; Huntingford et al., 2008; Gloor et al., 2013). Recent Amazonian droughts have gained particular attention due to the sensitivity of the tropical forest λE to climate change (Hilker et al., 2014). If persistent precipitation extremes become more prevalent (Hilker et al., 2014), the Amazon rainforest may increasingly become a net source of carbon as a result of both the suppression of net biome exchange by drought and carbon emissions from fires (Gatti et al., 2014). Changes in land cover due to conversion of tropical forest to pastures significantly alter the energy partitioning by decreasing λE and increasing sensible heat fluxes (H) over pasture sites (e.g., Priante Filho et al., 2004). This will ultimately lead to severe consequences for the water balance in the region, with changes to river discharge already observed in some parts of the basin (Davidson et al., 2012). Evaluating the λE response to changing climate and land use in the Amazon Basin is critical to understanding the stability of the tropics within the Earth system (Lawrence and Vandecar, 2015). The control of λE can be viewed as complex supply–demand interactions, where net radiation and soil moisture represent the supply and the atmospheric vapor pressure deficit represents the demand. This supply–demand interaction accelerates the biophysical feedbacks in λE, and understanding these biophysical feedbacks is necessary to assess the terrestrial biosphere response to water availability. Therefore, quantifying the critical role of biophysical variables on λE will add substantial insight to assessments of the resilience of the Amazon Basin under global change.

The aerodynamic and canopy conductances (g_A and g_C hereafter) (unit $m\,s^{-1}$) are the two most important biophysical variables regulating the evaporation (λE_E) and transpiration (λE_T) flux components of λE (Monteith and Unsworth, 2008; Dolman et al., 2014; Raupach, 1995; Colaizzi et al., 2012; Bonan et al., 2014). While g_A controls the bulk aerodynamic transfer of energy and water through the near-surface boundary layer, g_C represents the restriction on water vapor flow through the aggregated conductance from stomata of the leaves, in the case of a vegetated surface. In the case of partial vegetation cover, g_C also includes the soil surface conductance for evaporation. At a small g_C / g_A ratio, the vapor pressure deficit close to the canopy source/sink height (D_0) approximates the atmospheric vapor pressure deficit (D_A) due to aerodynamic mixing and/or low transpiration. This results in a strong canopy–atmosphere coupling, and such conditions are prevalent under soil moisture deficits, which prevails under conditions of soil moisture deficit. By contrast, a large g_C / g_A ratio influences the gradients of vapor pressure deficit just above the canopy, such that D_0 tends towards zero and thus remains different from D_A (Jarvis and McNaughton, 1986). This situation reflects a weak canopy–atmosphere coupling, and such situations prevail under predominantly wet conditions and/or poor aerodynamic mixing due to wetness-induced low aerodynamic roughness. The Penman–Monteith (PM) equation is a physically based scheme for quantifying such biophysical controls on canopy-scale λE_E and λE_T from terrestrial ecosystems, treating the vegetation canopy as "big-leaf" (Monteith, 1965, 1981). Despite its development based on biophysical principles controlling water vapor exchange, quantifying the g_A and g_C controls on λE through the PM equation suffers from the continued longstanding uncertainty in the aggregated stomatal and aerodynamic behavior within the soil–plant–atmosphere continuum (Matheny et al., 2014; Prihodko et al., 2008).

One of the major sources of uncertainties in modeling g_A is associated with the empirical (and uncertain) parameterizations of near-surface boundary-layer dynamics, which is invariably confounded by space–time variability in atmospheric stability (van der Tol et al., 2009; Shuttleworth, 1989; Gibson et al., 2011). For example, the Monin–Obukhov similarity theory (MOST) used for g_A modeling appears to be only valid over uniform, extensive, and flat surfaces (Monteith and Unsworth, 2008; van der Tol et al., 2009; Holwerda et al., 2012), and its application to complex "real" canopy systems is problematic due to chaotic interactions between turbulence, canopy roughness, and topography (Raupach and Finnigan, 1995; Shuttleworth, 2007; Holwerda et al., 2012). Similarly, g_C varies in space and time due to variations in plant species, photosynthetic capacity, soil moisture variability, and environmental drivers (Monteith and Unsworth, 2008; van der Tol et al., 2009). Despite the existence of several semi-mechanistic and empirical parameterizations for g_C (e.g., Ball et al., 1987; Leuning, 1995; Tuzet et al., 2003; Medlyn et al., 2011), the adaptive tendencies of plant canopies severely compromise the efficacy of such approaches (Matheny et al., 2014), limiting their applicability over most landscapes. Thus, debate on the most appropriate model for the canopy conductance has endured for decades.

Previous studies in the Amazon Basin focused on developing an observational understanding of the biogeochemical cycling of energy, water, carbon, trace gases, and aerosols in Amazonia (Andreae et al., 2002; Malhi et al., 2002; da Rocha et al., 2009), model-based understanding of surface ecophysiological behavior and seasonality of λE (Baker et al., 2013; Christoffersen et al., 2014), modeling the environmental controls on λE (Hasler and Avissar, 2007; Costa et al., 2010), understanding the seasonality of photosynthesis and of λE (da Rocha et al., 2004; Restrepo-Coupe et al., 2013), and the impact of land use on hydrometeorology (Roy and Avissar, 2002; von Randow et al., 2012). However, the combination of climatic and ecohydrological disturbances will significantly affect stomatal functioning, the partitioning of $\lambda E_{\mathrm{E}} - \lambda E_{\mathrm{T}}$, and carbon–water–climate interactions of tropical vegetation (Cox et al., 2000; Mercado et al., 2009). Hence, investigation of the effects of drought and land cover changes on conductances, λE_{E} and λE_{T}, is a topic requiring urgent attention (Blyth et al., 2010) both because of the cursory way it is handled in the current generation of parametric models (Matheny et al., 2014) and because of the centrality of g_{A} and g_{C} in controlling modeled flux behaviors (Villagarcía et al., 2010). The persistent risk of deforestation is likely to alter the radiation interception, surface temperature, surface moisture, associated meteorological conditions, and vegetation biophysical states of different plant functional types (PFTs). Conversion from forest to pasture is expected to change the $g_{\mathrm{C}}/g_{\mathrm{A}}$ ratio of these ecosystems and impact the evapotranspiration components. Besides inverting the PM equation using field measurements of λE, to date either photosynthesis-dependent modeling or leaf-scale experiments were performed to directly quantify g_{C} (Ball et al., 1987; Meinzer et al., 1993, 1997; Monteith, 1995; Jones, 1998; Motzer et al., 2005). However, an analytical or physical retrieval for g_{A} and g_{C} is required not only to better understand the role of the canopy in regulating evaporation and transpiration, but also to enable our capability to characterize the conductances using remote observations, across large spatial domains where in situ observations are not available. This paper aims to leverage this emerging opportunity by exploring data from the Large-scale Biosphere-Atmosphere Experiment in Amazonia (LBA) eddy covariance (EC) observations (e.g., de Goncalves et al., 2013; Restrepo-Coupe et al., 2013) using a novel analytical modeling technique, the Surface Temperature Initiated Closure (STIC) (Mallick et al., 2014, 2015), in order to quantify the biophysical control on λE_{E} and λE_{T} over several representative PFTs of the Amazon Basin.

STIC (STIC1.0 and STIC1.1) provides a unique framework for simultaneously estimating g_{A} and g_{C}, surface energy balance fluxes, and λE_{E} and λE_{T}. It is based on finding analytical solutions for g_{A} and g_{C} by physically integrating radiometric surface temperature (T_{R}) information (along with radiative fluxes and meteorological variables) into the PM model (Mallick et al., 2014, 2015). The direct estimates of canopy-scale conductances and λE obtained through STIC are independent of any land surface parameterization. This contrasts with the multi-layer canopy models that explicitly parameterize the leaf-scale conductances and perform bottom-up scaling to derive the canopy-scale conductances (Baldocchi et al., 2002; Drewry et al., 2010). A primary advantage of the approach on which STIC is based is the ability to directly utilize remotely sensed T_{R} to estimate E, thereby providing a capability to estimate E over large spatial scales using a remotely sensed variable that is central to many ongoing and upcoming missions. This study presents a detailed examination of the performance of STIC to better understand land–atmosphere interactions in one of the most critical global ecosystems and addresses the following science questions and objectives.

1. How realistic are canopy-scale conductances when estimated analytically (or non-parametrically) without involving any empirical leaf-scale parameterization?
2. What are the controls of canopy-scale g_{A} and g_{C} on evaporation and transpiration in the Amazon Basin, as evaluated using STIC?
3. How do the STIC-based canopy-scale conductances compare with known environmental constraints?
4. Is the biophysical response of g_{C} consistent with the leaf-scale theory (Jarvis and McNaughton, 1986; McNaughton and Jarvis, 1991; Monteith, 1995)?

The following section describes a brief methodology to retrieve g_{C}, g_{A}, λE_{E}, and λE_{T}. The data sources used for the analysis are described after the methodology and will be followed by a comparison of the results with fluxes derived from EC measurements. A detailed discussion of the results and potential applicability of the method with implications for global change research are elaborated at the end. A list of symbols and variables used in the present study is given in Table 1.

2 Methodology

2.1 Theory

The retrievals of g_{A}, g_{C}, and λE are based on finding a "closure" of the PM equation (Eq. 1 below) using the STIC framework (Fig. A1) (Mallick et al., 2015). STIC is a physically based single-source surface energy balance scheme that includes internally consistent estimation of g_{A} and g_{C} (Mallick et al., 2014, 2015). Originally designed for application to thermal remote sensing data from Earth observation sensors, the STIC framework exploits observations of radiative (T_{R}) and environmental variables, including net radiation (R_{N}), ground heat flux (G), air temperature (T_{A}), relative humidity (R_{H}), or vapor pressure (e_{A}) at a reference level above the surface.

Table 1. Variables and symbols and their description used in the present study.

Variables and symbols	Description
λE	Evapotranspiration (evaporation + transpiration) as latent heat flux ($W\,m^{-2}$)
H	Sensible heat flux ($W\,m^{-2}$)
R_N	Net radiation ($W\,m^{-2}$)
G	Ground heat flux ($W\,m^{-2}$)
ϕ	Net available energy ($W\,m^{-2}$)
T_A	Air temperature (°C)
T_D	Dew-point temperature (°C)
T_R	Radiometric surface temperature (°C)
R_H	Relative humidity (%)
e_A	Atmospheric vapor pressure at the level of T_A measurement (hPa)
D_A	Atmospheric vapor pressure deficit at the level of T_A measurement (hPa)
u	Wind speed ($m\,s^{-1}$)
u^*	Friction velocity ($m\,s^{-1}$)
T_{SD}	Dew-point temperature at the source/sink height (°C)
T_0	Aerodynamic temperature or source/sink height temperature (°C)
e_S	"Effective" vapor pressure of evaporating front near the surface (hPa)
e_S^*	Saturation vapor pressure of the surface (hPa)
e_0^*	Saturation vapor pressure at the source/sink height (hPa)
e_0	Atmospheric vapor pressure at the source/sink height (hPa)
D_0	Atmospheric vapor pressure deficit at the source/sink height (hPa)
λE_{eq}	Equilibrium latent heat flux ($W\,m^{-2}$)
λE_{imp}	Imposed latent heat flux ($W\,m^{-2}$)
λE_E	Evaporation as flux ($W\,m^{-2}$)
λE_T	Transpiration as flux ($W\,m^{-2}$)
E	Evapotranspiration (evaporation + transpiration) as depth of water (mm)
λE^*	Potential evaporation as flux ($W\,m^{-2}$)
λE_T^*	Potential transpiration as flux ($W\,m^{-2}$)
λE_W	Wet environment evaporation as flux ($W\,m^{-2}$)
λE_P^*	Potential evaporation as flux according to Penman ($W\,m^{-2}$)
λE_{PM}^*	Potential evaporation as flux according to Penman–Monteith ($W\,m^{-2}$)
λE_{PT}^*	Potential evaporation as flux according to Priestley–Taylor ($W\,m^{-2}$)
E^*	Potential evaporation as depth of water (mm)
E_P^*	Potential evaporation as depth of water according to Penman (mm)
E_{PM}^*	Potential evaporation as depth of water according to Penman–Monteith (mm)
E_{PT}^*	Potential evaporation as depth of water according to Priestley–Taylor (mm)
E_W	Wet environment evaporation as depth of water (mm)
g_A	Aerodynamic conductance ($m\,s^{-1}$)
g_C	Stomatal/surface conductance ($m\,s^{-1}$)
g_M	Momentum conductance ($m\,s^{-1}$)
g_B	Quasi-laminar boundary-layer conductance ($m\,s^{-1}$)
g_{Cmax}	Maximum stomatal/surface conductance ($m\,s^{-1}$) ($= g_C/M$)
M	Surface moisture availability (0–1)
s	Slope of saturation vapor pressure vs. temperature curve ($hPa\,K^{-1}$) (estimated at T_A)
s_1	Slope of the saturation vapor pressure and temperature between ($T_{SD} - T_D$) vs. ($e_0 - e_A$) (approximated at T_D) ($hPa\,K^{-1}$)
s_2	Slope of the saturation vapor pressure and temperature between ($T_R - T_D$) vs. ($e_S^* - e_A$) ($hPa\,K^{-1}$), estimated according to Mallick et al. (2015)
s_3	Slope of the saturation vapor pressure and temperature between ($T_R - T_{SD}$) vs. ($e_S^* - e_S$) (approximated at T_R) ($hPa\,K^{-1}$)
k	Ratio between ($e_0^* - e_A$) and ($e_S^* - e_A$)
λ	Latent heat of vaporization of water ($J\,kg^{-1}\,K^{-1}$)
z_R	Reference height (m)

Table 1. Continued.

Variables and symbols	Description
z_M	Effective source–sink height of momentum (m)
z_0	Roughness length (m)
d	Displacement height (m)
γ	Psychrometric constant (hPa K^{-1})
ρ	Density of air (kg m^{-3})
c_p	Specific heat of dry air (MJ kg^{-1} K^{-1})
Λ	Evaporative fraction (unitless)
β	Bowen ratio (unitless)
α	Priestley–Taylor parameter (unitless)
Ω	Decoupling coefficient (unitless)
Sc	Schmidt number (unitless)
Pr	Prandtl number (unitless)
κ	von Kármán constant (0.4)

The foundation of the development of STIC is based on the goal of finding an analytical solution of the two unobserved "state variables" (g_A and g_C) in the PM equation while exploiting the radiative (R_N and G), meteorological (T_A, R_H), and radiometric surface temperature (T_R) as external inputs. The fundamental assumption in STIC is the first-order dependence of g_A and g_C on the aerodynamic temperature (T_0) and soil moisture (through T_R). This assumption allows a direct integration of T_R into the PM equation while simultaneously constraining the conductances through T_R. Although the T_R signal is implicit in R_N, which appears in the numerator of the PM equation (Eq. 1), it may be noted that R_N has a relatively weak dependence on T_R (compared to the sensitivity of T_R to soil moisture and λE). Given that T_R is a direct signature of the soil moisture availability, inclusion of T_R in the PM equation also works to add water-stress controls in g_C. Until now the explicit use of T_R in the PM model was hindered due to the unavailability of any direct method to integrate T_R into this model, and, furthermore, due to the lack of physical models expressing biophysical states of vegetation as a function of T_R. Therefore, the majority of the PM-based λE modeling approaches strongly rely on surface reflectance and meteorology while exploiting the empirical leaf-scale parameterizations of the biophysical conductances (Prihodko et al., 2008; Bonan et al., 2014; Ershadi et al., 2015).

The PM equation is commonly expressed as

$$\lambda E = \frac{s\phi + \rho\, c_P\, g_A D_A}{s + \gamma\left(1 + \frac{g_A}{g_C}\right)}, \tag{1}$$

where ρ is the air density (kg m^{-3}), c_P is the specific heat of air (J kg^{-1} K^{-1}), γ is the psychrometric constant (hPa K^{-1}), s is the slope of the saturation vapor pressure vs. air temperature (hPa K^{-1}), D_A is the saturation deficit of the air (hPa) or vapor pressure deficit at the reference level, and ϕ is the net available energy (W m^{-2}) (the difference between R_N and G). The units of all the surface fluxes and conductances are in W m^{-2} and m s^{-1}, respectively. For a dense canopy, g_C in the PM equation represents the canopy surface conductance. Although it is not equal to the canopy stomatal conductance, it contains integrated information on the stomata. For a heterogeneous landscape, g_C in the PM equation is an aggregated surface conductance containing information on both canopy and soil. Traditionally, the two unknown "state variables" in Eq. (1) are g_A and g_C, and the STIC methodology is based on formulating "state equations" for these conductances that satisfy the PM model (Mallick et al., 2014, 2015). The PM equation is "closed" upon the availability of canopy-scale measurements of the two unobserved biophysical conductances, and if we assume the empirical models of g_A and g_C to be reliable. However, neither g_A nor g_C can be measured at the canopy scale or at larger spatial scales. Furthermore, as shown by some recent studies (Matheny et al., 2014; Van Dijk et al., 2015), a more appropriate g_A and g_C model is currently not available. This implies that a true "closure" of the PM equation is only possible through an analytical estimation of the conductances.

2.2 State equations

By integrating T_R with standard surface energy balance (SEB) theory and vegetation biophysical principles, STIC formulates multiple "state equations" that eliminate the need for exogenous parametric submodels for g_A and g_C, associated aerodynamic variables, and land–atmosphere coupling. The state equations of STIC are as follows and their detailed derivations are described in Appendix A1.

$$g_A = \frac{\phi}{\rho c_P\left[(T_0 - T_A) + \left(\frac{e_0 - e_A}{\gamma}\right)\right]} \tag{2}$$

$$g_C = g_A \frac{(e_0 - e_A)}{(e_0^* - e_0)} \tag{3}$$

$$T_0 = T_A + \left(\frac{e_0 - e_A}{\gamma}\right)\left(\frac{1-\Lambda}{\Lambda}\right) \tag{4}$$

$$\Lambda = \frac{2\alpha s}{2s + 2\gamma + \gamma\frac{g_A}{g_C}(1+M)} \tag{5}$$

Here, T_0 is the temperature (°C) at the source/sink height (or at the roughness length (z_0) or in-canopy air stream), e_0 is the atmospheric vapor pressure (hPa) at the source/sink height, e_0^* is the saturation vapor pressure (hPa) at the source/sink height, Λ is the evaporative fraction (the ratio of λE and ϕ), α is the Priestley–Taylor parameter (unitless) (Priestley and Taylor, 1972), and M is a unitless quantity that describes the relative wetness (or moisture availability) of the surface. M controls the transition from potential to actual evaporation and hence is critical for providing a constraint against which the conductances can be estimated (M estimation is

explained in Appendix A2). Given values of R_N, G, T_A, and R_H or e_A, the four state equations (Eqs. 2–5) can be solved simultaneously to derive analytical solutions for the four state variables. This also produces a "closure" of the PM model, which is independent of empirical parameterizations for both g_A and g_C. However, the analytical solutions to the above state equations have four accompanying unknowns, M (surface moisture availability), e_0 (vapor pressure at the source/sink height), e_0^* (saturation vapor pressure at the source/sink height), and the Priestley–Taylor coefficient (α), and as a result there are four equations with eight unknowns. Consequently an iterative solution is needed to determine the four unknown variables (as described in Appendix A2), which is a further modification of the STIC1.1 framework (Mallick et al., 2015). The present version of STIC is designated as STIC1.2 and its uniqueness is the physical integration of T_R into a combined structure of the PM and Shuttleworth–Wallace (SW, hereafter) (Shuttleworth and Wallace, 1985) models to estimate the source/sink height vapor pressures (Appendix A2). In addition to physically integrating T_R observations into a combined PM–SW framework, STIC1.2 also establishes a feedback loop describing the relationship between T_R and λE, coupled with canopy–atmosphere components relating λE to T_0 and e_0. To estimate M, the radiometric surface temperature (T_R) is extensively used in a physical retrieval framework, thus treating T_R as an external input. In Eq. (5), the Priestley–Taylor coefficient (α) appeared due to the use of the advection–aridity (AA) hypothesis (Brutsaert and Stricker, 1979) for deriving the state equation of Λ (Supplement S1). However, instead of optimizing α as a "fixed parameter", we have developed a physical equation of α (Eq. A15) and numerically estimated α as a "variable". The derivation of the equation for α is described in Appendix A2. The fundamental differences between STIC1.2 and earlier versions are described in Table A1.

In STIC1.2, T_0 is a function of T_R, and they are not assumed equal ($T_0 \neq T_R$). The analytical expression of T_0 is dependent on M and the estimation of M is based on T_R. To further elaborate this point on the inequality of T_0 and T_R, we show an intercomparison of retrieved T_0 vs. T_R for forest and pasture (Fig. A2). This indicates the distinct difference of the retrieved T_0 from T_R for the two different biomes.

2.3 Partitioning λE

The terrestrial latent heat flux is an aggregate of both transpiration (λE_T) and evaporation (λE_E) (sum of soil evaporation and interception evaporation from the canopy). During rain events the land surface becomes wet and λE tends to approach the potential evaporation (λE^*), while surface drying after rainfall causes λE to approach the potential transpiration rate (λE_T^*) in the presence of vegetation, or zero without any vegetation. Hence, λE at any time is a mixture of these two end-member conditions depending on the degree of surface moisture availability or wetness (M) (Bosveld and Bouten, 2003; Loescher et al., 2005). Considering the general case of evaporation from an unsaturated surface at a rate less than the potential, M is the ratio of the actual to potential evaporation rate and is considered as an index of evaporation efficiency during a given time interval (Boulet et al., 2015). Partitioning of λE into λE_E and λE_T was performed according to Mallick et al. (2014) as follows:

$$\lambda E = \lambda E_E + \lambda E_T = M\lambda E^* + (1 - M)\lambda E_T^*. \quad (6)$$

The estimates of λE_E in the current method consist of an aggregated contribution from both interception and soil evaporation, and no further attempt is made to separate these two components. In the Amazon forest, soil evaporation has a negligible contribution, while the interception evaporation contributes substantially to the total evaporative fluxes, and therefore the partitioning of λE into λE_E and λE_T is crucial. After estimating g_A, λE^* was estimated according to the Penman equation (Penman, 1948) and λE_T was estimated as the residual in Eq. (6).

In this study, we use the term "canopy conductance" instead of "stomatal conductance" given that the term "stomata" is applicable at the leaf scale only. As stated earlier, for a heterogeneous surface, g_C should principally be a mixture of the canopy surface (integrated stomatal information) and soil conductances. However, given the high vegetation density of the Amazon Basin, the soil surface exposure is negligible, and hence we assume g_C to be the canopy-scale aggregate of the stomatal conductance. Similarly, a different g_A exists for soil–canopy, sun–shade, and dry–wet conditions (Leuning, 1995), which are currently integrated into a lumped g_A (given the big-leaf nature of STIC). From the big-leaf perspective, it is generally assumed that the aerodynamic conductance of water vapor and heat are equal (Raupach, 1998). However, to obtain partitioned aerodynamic conductances, explicit partitioning of λE is needed, which is beyond the scope of the current paper.

2.4 Evaluating g_A and g_C

Due to the lack of direct canopy-scale g_A measurements, a rigorous evaluation of g_A cannot be performed. To evaluate the STIC retrievals of g_A ($g_{A\text{-STIC}}$), we adopted three different methods.

a. By using the measured friction velocity (u^*) and wind speed (u) at the EC towers and using the equation of Baldocchi and Ma (2013) ($g_{A\text{-BM13}}$) in which g_A was expressed as the sum of turbulent conductance and canopy (quasi-laminar) boundary-layer conductance as

$$g_{A\text{-BM13}} = \left[\left(u/u^{*2}\right) + \left(2/ku^{*2}\right)(Sc/Pr)^{0.67}\right]^{-1}, \quad (7)$$

where κ is the von Kármán constant, 0.4; Sc is the Schmidt number; Pr is the Prandtl number, and their

ratio is generally considered to be unity. Here the conductances of momentum, sensible, and latent heat fluxes are assumed to be identical (Raupach, 1998).

b. By inverting λE observations for wet conditions, hence assuming $\lambda E \cong \lambda E^*$ and estimating g_A ($g_{A\text{-INV}}$) as

$$g_{A\text{-INV}} = \gamma \lambda E / \rho c_P D_A. \quad (8)$$

c. By inverting the aerodynamic equation of H and estimating a hybrid g_A ($g_{A\text{-HYB}}$) from observed H and STIC T_0 as ($T_{0\text{-STIC}}$),

$$g_{A\text{-HYB}} = H / \rho c_P \left(T_{0\text{-STIC}} - T_A\right). \quad (9)$$

Like $g_{A\text{-STIC}}$, direct verification of STIC g_C ($g_{C\text{-STIC}}$) could not be performed, as canopy-scale g_C observations are not possible with current measurement techniques. Although leaf-scale g_C measurements are relatively straightforward, these values are not comparable to values retrieved at the canopy scale. However, assuming u^*-based g_A as the baseline aerodynamic conductance, we have estimated canopy-scale g_C by inverting the PM equation ($g_{C\text{-INV}}$) (Monteith, 1995) to evaluate $g_{C\text{-STIC}}$ by exploiting $g_{A\text{-BM13}}$ in conjunction with the available ϕ, λE, T_A, and D_A measurements from the EC towers.

2.5 Decoupling coefficient and biophysical controls

The decoupling coefficient or "Omega" (Ω) is a dimensionless coefficient ranging from 0.0 to 1.0 (Jarvis and McNaughton, 1986) and is considered as an index of the degree of stomatal control on transpiration relative to the environment. The equation of Ω is as follows:

$$\Omega = \frac{\frac{s}{\gamma} + 1}{\frac{s}{\gamma} + 1 + \frac{g_A}{g_C}}. \quad (10)$$

Introducing Ω into the Penman–Monteith (PM) equation for λE results in

$$\lambda E = \Omega \lambda E_{eq} + (1 - \Omega) \lambda E_{imp}, \quad (11)$$

$$\lambda E_{eq} = \frac{s\phi}{s + \gamma}, \quad (12)$$

$$\lambda E_{imp} = \frac{\rho c_P}{\gamma} g_C D_A, \quad (13)$$

where λE_{eq} is the equilibrium latent heat flux, which depends only on ϕ and would be obtained over an extensive surface of uniform moisture availability (Jarvis and McNaughton, 1986; Kumagai et al., 2004). λE_{imp} is the imposed latent heat flux, which is "imposed" by the atmosphere on the vegetation surface through the effects of vapor pressure deficit (triggered under limited soil moisture availability), and λE becomes proportional to g_C.

When the g_C/g_A ratio is very small (i.e., water-stress conditions), stomata principally control the water loss, and a change in g_C will result in a nearly proportional change in transpiration. Such conditions trigger a strong biophysical control on transpiration. In this case the Ω value approaches zero and vegetation is believed to be fully coupled to the atmosphere. In contrast, for a high g_C / g_A ratio (i.e., high water availability), changes in g_C will have little effect on the transpiration rate, and transpiration is predominantly controlled by ϕ. In this case the Ω value approaches unity, and vegetation is considered to be poorly coupled to the atmosphere.

Given that both g_A and g_C are the independent estimates in STIC1.2, the concept of Ω was used to understand the degree of biophysical control on λE_T, which indicates the extent to which the transpiration fluxes are approaching the equilibrium limit. However, the biophysical characterization of λE_T and λE_E through STIC1.2 significantly differs from previous approaches (Ma et al., 2015; Chen et al., 2011; Kumagai et al., 2004), and the fundamental differences are centered on the specifications of g_A and g_C (as described in Table A2). While the estimation of g_A in previous approaches was based on u and u^*, the estimation of g_C was based on inversion of observed λE based on the PM equation (e.g., Stella et al., 2013). However, none of these approaches allow independent quantification of biophysical controls of λE, as g_C is constrained by λE itself.

3 Datasets

Eddy covariance and meteorological quantities

We used the LBA (Large-Scale Biosphere-Atmosphere Experiment in Amazonia) data for quantifying the biophysical controls on the evaporative flux components. LBA was an international research initiative conducted during 1995–2005 to study how Amazonia functions as a regional entity within the larger Earth system, and how changes in land use and climate will affect the hydrological and biogeochemical functioning of the Amazon ecosystem (Andreae et al., 2002).

A network of eddy covariance (EC) towers was operational during the LBA experiment, such that data from nine EC towers were obtained from the ORNL Distributed Archive Active Centre (ftp://daac.ornl.gov/data/lba/carbon_dynamics/CD32_Brazil_Flux_Network/). These are the quality-controlled and harmonized surface flux and meteorological data from the Brazilian Amazon flux network. Time series of surface fluxes (λE, H, G), radiation (R_N, shortwave and longwave), thermal (T_R), meteorological quantities (T_A, R_H, wind speed) as well as soil moisture and rainfall were available from six (out of nine) EC towers. Three of the EC towers had numerous missing data and were not included in the analysis. The surface energy balance was closed by applying the Bowen ratio (Bowen, 1926) closure as described in Chavez et al. (2005) and later

Table 2. Overview of the LBA tower sites. Here, (–) refers to (S) and (W) for latitude and longitude, respectively.

Biome	PFT	Site	LBA code	Data availability period	Latitude (°)	Longitude (°)	Tower height (m)	Annual rainfall (mm)
Forest	Tropical rainforest (TRF)	Manaus KM34	K34	Jun 1999 to Sep 2006	−2.609	−60.209	50	2329
Forest	Tropical moist forest (TMF)	Santarem KM67	K67	Jan 2002 to Jan 2006	−2.857	−54.959	63	1597
Forest	Tropical moist forest (TMF)	Santarem KM83	K83	Jul 2000 to Dec 2004	−3.018	−54.971	64	1656
Forest	Tropical dry forest (TDF)	Reserva Biológica Jarú	RJA	Mar 1999 to Oct 2002	−10.083	−61.931	60	2354
Pasture	Pasture (PAS)	Santarem KM77	K77	Jan 2000 to Dec 2001	−3.012	−54.536	18	1597
Pasture	Pasture (PAS)	Fazenda Nossa Senhora	FNS	Mar 1999 to Oct 2002	−10.762	−62.357	8.5	1743

adopted by Anderson et al. (2007) and Mallick et al. (2015). In the absence of G measurements, ϕ was assumed to be equal to the sum of λE and H with the assumption that a dense vegetation canopy restricts the energy incident on the soil surface, thereby allowing us to assume negligible ground heat flux. For the present analysis, data from six selected EC towers (Table 2) represent two different biomes (forest and pasture) covering four different PFTs, namely, tropical rainforest (TRF), tropical moist forest (TMF), tropical dry forest (TDF), and pasture (PAS), respectively. A general description of the datasets can be found in Saleska et al. (2013). For all sites, monthly averages of the diurnal cycle (hourly time resolution) were chosen for the present analysis.

4 Results

4.1 Evaluating g_A, g_C, and surface energy balance fluxes

Examples of monthly averages of the diurnal cycles of the four different g_A estimates and their corresponding g_C estimates over two different PFTs (K34 for forest and FNS for pasture) reveal that $g_{A\text{-STIC}}$ and $g_{C\text{-STIC}}$ tend to be generally higher for the forest than their counterparts, varying from 0 to $0.06\,m\,s^{-1}$ and 0 to $0.04\,m\,s^{-1}$ respectively (Fig. 1a and b). The magnitude of $g_{A\text{-STIC}}$ varied between 0 and $0.025\,m\,s^{-1}$ for the pasture (Fig. 1a), while $g_{C\text{-STIC}}$ values were less than half of those estimated over the forest (0–$0.01\,m\,s^{-1}$) (Fig. 1b). The conductances showed a marked diurnal variation expressing their overall dependence on net radiation, vapor pressure deficit, and surface temperature. Despite the absolute differences between the conductances from the different retrieval methods, their diurnal patterns were comparable.

The canopy-scale evaluation of $g_{A\text{-STIC}}$ is illustrated in Fig. 2a (and Table 3), combining data from the four PFTs. Estimated values range between zero and $0.1\,m\,s^{-1}$ and show modest correlation ($R^2 = 0.44$) (R^2 range between 0.22 [±0.18] and 0.55 [±0.12]) between $g_{A\text{-BM13}}$ and $g_{A\text{-STIC}}$, with regression parameters ranging from 0.81 (±0.023) to 1.07 (±0.047) for the slope and 0.0019 (±0.0006) to 0.0006 (±0.0006) $m\,s^{-1}$ for the offset (Table 3). The root mean squared deviation (RMSD) varied between 0.007 (TDF) and $0.013\,m\,s^{-1}$ (TRF). Statistical comparisons between $g_{A\text{-STIC}}$ and $g_{A\text{-HYB}}$ revealed relatively low RMSD and high correlation between them (RMSD = $0.007\,m\,s^{-1}$ and $R^2 = 0.77$) as compared to the error statistics between $g_{A\text{-STIC}}$ and $g_{A\text{-INV}}$ (RMSD = $0.011\,m\,s^{-1}$ and $R^2 = 0.50$) (Fig. 2b and c). The residuals between $g_{A\text{-STIC}}$ and $g_{A\text{-BM13}}$ are plotted as a function of u and u^* in Fig. 2d with the aim of ascertaining whether significant biases are introduced by ignoring wind and shear information within STIC1.2. As illustrated in Fig. 2d, there appears to be a weak systematic relation-

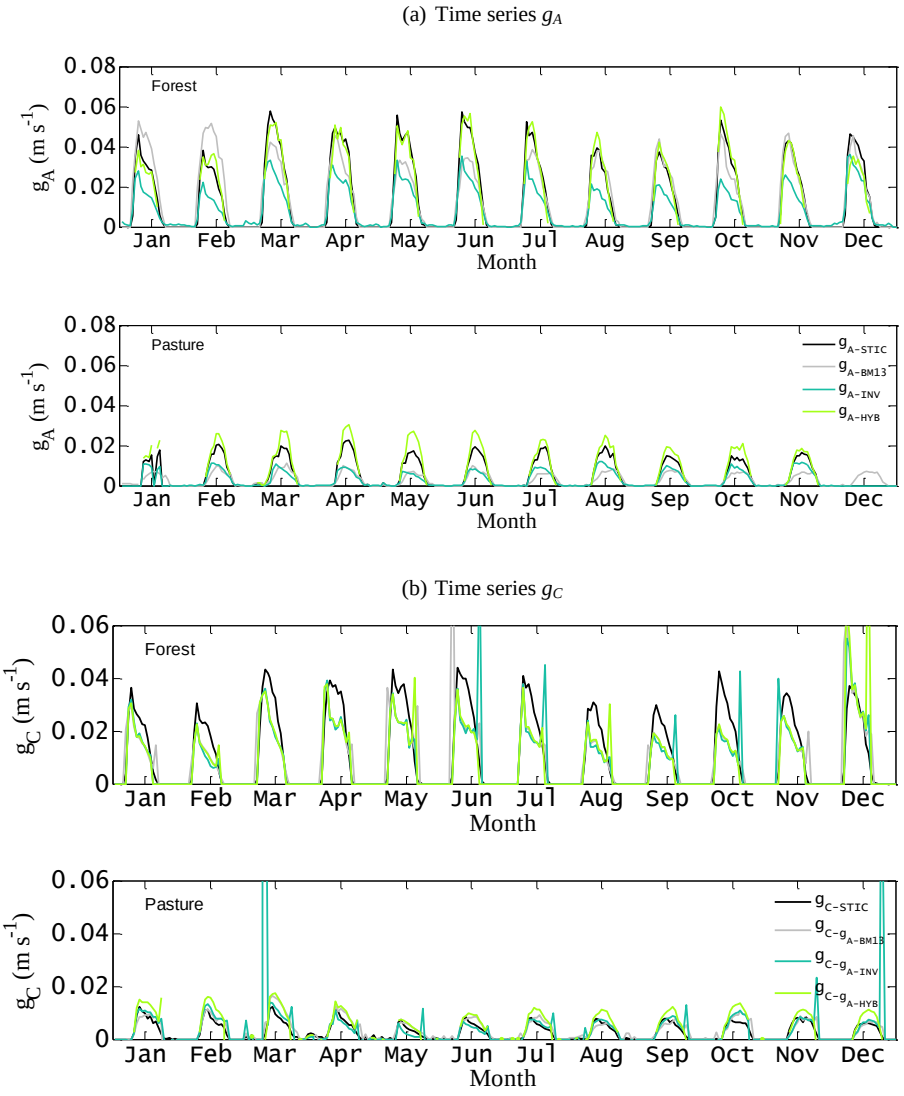

Figure 1. Examples of monthly averages of the diurnal time series of canopy-scale **(a)** g_A and **(b)** g_C estimated for two different biomes (forest and pasture) in the Amazon Basin (LBA sites K34 and FNS). The time series of four different g_A estimates and their corresponding g_C estimates are shown here.

ship between the residual g_A difference with either u^* or u ($r = -0.26$ and -0.17). However, a considerable relationship was found between wind- and shear-driven g_A (i.e., $g_{A\text{-BM13}}$) vs. ϕ, T_R, and D_A ($r = 0.83$, 0.48, and 0.42) (Fig. 2e and f), which indicates that these three energy and water constraints can explain 69, 23, and 17 % variance of $g_{A\text{-BM13}}$, respectively.

Canopy-scale evaluation of hourly g_C is presented in Fig. 3a (and Table 3), combining data from the four PFTs. Estimated values range between zero and 0.06 m s^{-1} for $g_{C\text{-STIC}}$ and show reasonable correlation ($R^2 = 0.39$) (R^2 range between 0.14 [±0.04] and 0.58 [±0.12]) between $g_{C\text{-STIC}}$ and $g_{C\text{-INV}}$, with regression parameters ranging between 0.30 (±0.022) and 0.85 (±0.025) for the slope and between 0.0024 (±0.0003) and 0.0097 (±0.0007) m s^{-1} for the offset (Table 3). The RMSD varied between 0.007 (PAS) and 0.012 m s^{-1} (TRF and TDF). Given that g_A significantly controls g_C, we also examined whether biases in g_C are introduced by ignoring wind and shear information within STIC. The scatter plots between the residual g_C difference ($g_{C\text{-STIC}} - g_{C\text{-INV}}$) vs. both u and u^* (Fig. 3b) showed g_C residuals to be evenly distributed across the entire range of u and u^*, and no systematic pattern was evident.

The reliability of STIC1.2-based g_A and g_C retrievals was further verified by evaluating λE and H estimates (Fig. 4). Both the predicted λE and H are generally in good agreement with the observations, with substantial correlation (r) (R^2 from 0.61 to 0.94), reasonable RMSD of 33 and 37 W m^{-2}, and mean absolute percent deviation (MAPD) of 14 and 32 % between the observed and STIC fluxes

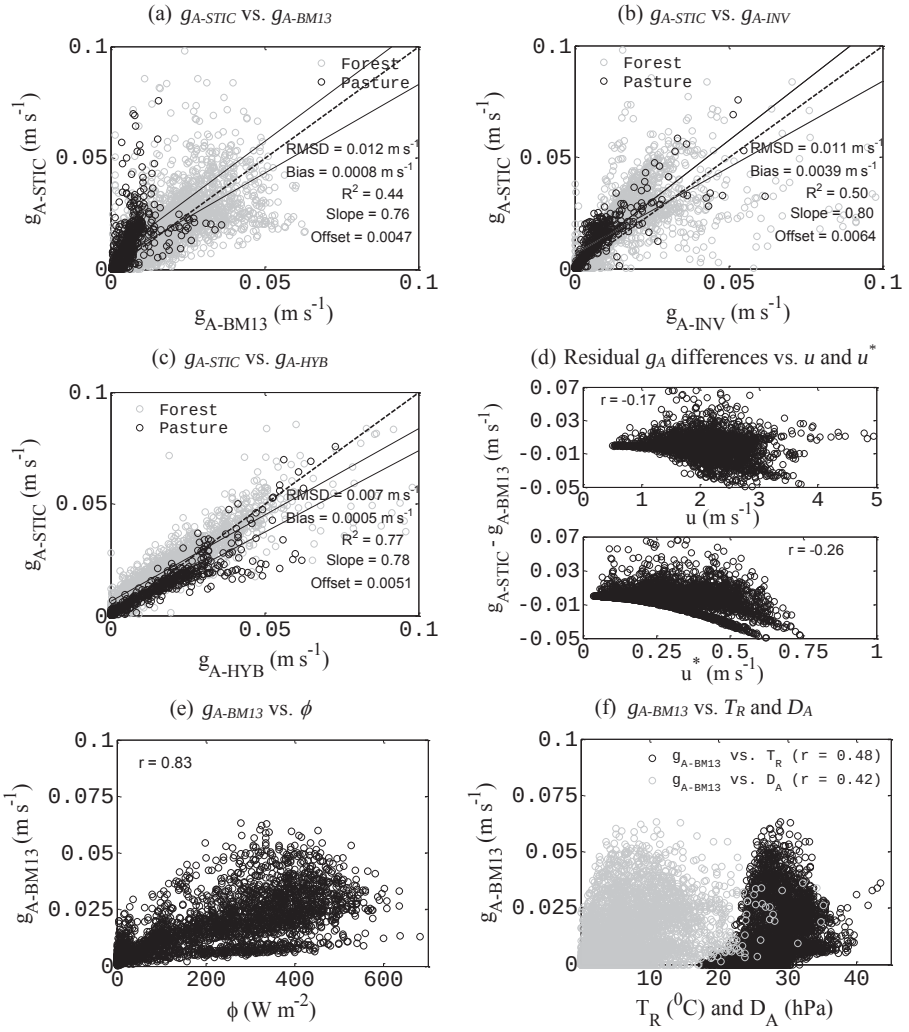

Figure 2. **(a)** Comparison between STIC-derived g_A ($g_{A\text{-STIC}}$) with an estimated aerodynamic conductance based on friction velocity (u^*) and wind speed (u) according to Baldocchi and Ma (2013) ($g_{A\text{-BM13}}$), **(b)** comparison between $g_{A\text{-STIC}}$ with an inverted g_A ($g_{A\text{-INV}}$) based on EC observations of λE and D_A, **(c)** comparison between $g_{A\text{-STIC}}$ with a hybrid g_A ($g_{A\text{-HYB}}$) based on EC observations of H and estimated T_0 over the LBA EC sites, **(d)** comparison between residual g_A differences vs. u and u^*, and **(e, f)** relationship between wind- and shear-derived g_A vs. ϕ, T_R, and D_A over the LBA EC sites.

(Fig. 4), respectively. Regression parameters varied between 0.96 (±0.008) and 1.14 (±0.010) for the slope and between −16 (±2) and −2 (±2) W m^{-2} for the offset for λE (Table 4), whereas for H, these were 0.60 (±0.025) to 0.89 (±0.035) for the slope and 9 (±1) to 29 (±2) W m^{-2} for the offset (Table 3), respectively. The RMSD in λE varied from 20 to 31 W m^{-2} and from 23 to 34 W m^{-2} for H (Table 3).

The evaluation of the conductances and surface energy fluxes indicates some efficacy for the STIC-derived fluxes and conductance estimates that represent a weighted average of these variables over the source area around the EC tower.

4.2 Canopy coupling, transpiration, and evaporation

From Fig. 5a an overall weak to moderate relationship ($r = -0.31$ to -0.42) is apparent between the coupling (i.e., $1 - \Omega$) and λE_T, where λE_T is negatively related to the coupling for all the PFTs, thus indicating the influence of weak to moderate biophysical controls on λE_T throughout the year in addition to radiative controls. The biophysical control was substantially enhanced in TRF (r increased from −0.36 to −0.53 and −0.60) (47 to 67 % increase) and TMF (r increased from −0.31 to −0.53 and −0.58) (70 to 85 % increase) during the dry seasons (July–September) (Fig. 5a). A profound increase in the biophysical control on λE_T during the dry season was also found in TDF (52 % increase) and PAS (37 % increase) (Fig. 5a). The negative relationship

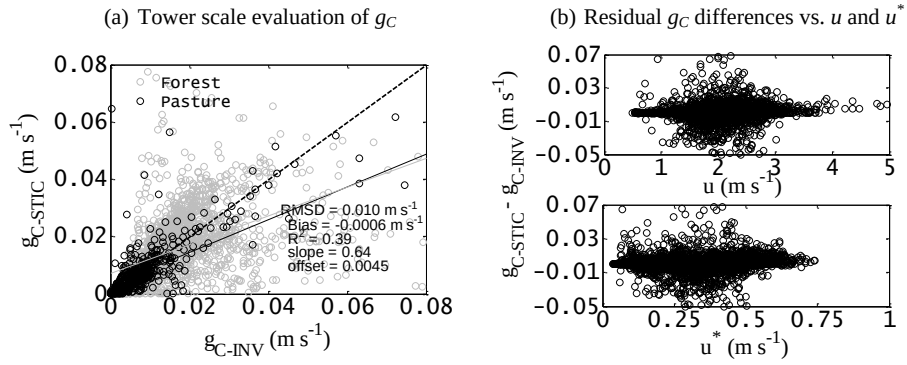

Figure 3. (a) Comparison between STIC-derived g_C ($g_{C\text{-STIC}}$) and g_C computed by inverting the PM model ($g_{C\text{-INV}}$) over the LBA EC sites, where $g_{A\text{-BM13}}$ was used as aerodynamic input in conjunction with tower measurements of λE, radiation and meteorological variables, and **(b)** residual g_C differences vs. wind speed (u) and friction velocity (u^*) over the LBA EC sites.

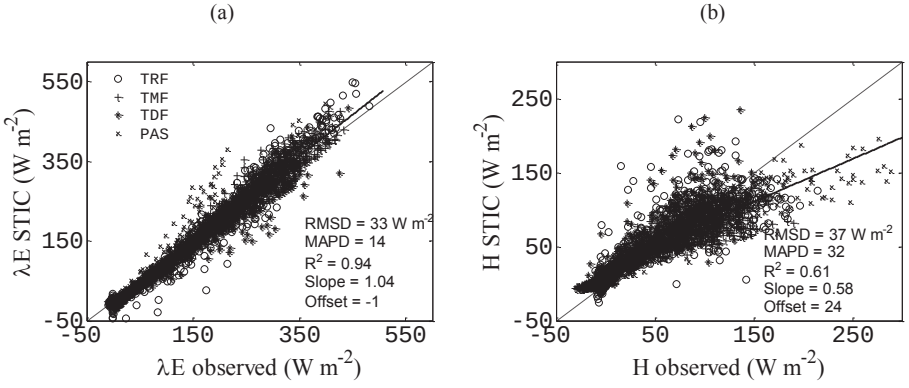

Figure 4. Comparison between STIC-derived **(a)** λE and **(b)** H over four different PFTs in the Amazon Basin (LBA tower sites). MAPD is the percent error defined as the mean absolute deviation between the predicted and observed variables divided by the mean observed variable.

($r = -0.29$ to -0.45) between $(1 - \Omega)$ and λE_E (Fig. 5b) in all four PFTs indicated the role of aerodynamic control on λE_E. The aerodynamic control was also enhanced during the dry seasons, as shown by the increased negative correlation ($r = -0.50$ to -0.69) (Fig. 5b) between $(1 - \Omega)$ and λE_E.

Illustrative examples of the diurnal variations of λE_E, λE_T, and Ω for two different PFTs with different annual rainfall (2329 mm in rainforest, K34, and 1597 mm in pasture, FNS) for 3 consecutive days during both dry and wet seasons are shown in Fig. 5c–f. This shows the morning rise of Ω and a near-constant afternoon Ω in the wet season (Fig. 5c and 5d), thus indicating no biophysical controls on λE_E and λE_T during this season. By contrast, during the dry season, the morning rise in Ω is followed by a decrease during noontime (15 to 25 % increase in coupling in forest and pasture) (Fig. 5e and f) due to dominant biophysical control, which is further accompanied by a transient increase from mid-afternoon till late afternoon, and steadily declines thereafter. Interestingly, coupling was relatively higher in pasture during the dry seasons, and the reasons are detailed in the following section and discussion.

4.3 g_C and g_A vs. transpiration and evaporation

Scatter plots between λE_T and λE_E vs. g_C and g_A showed a triangular pattern that became wider with increasing conductances (Fig. 6). To explain this behavior of λE_T vs. g_C and g_A, we further examined the entire mechanism of conductance–λE_T interactions through two-dimensional scatters between λE_T and conductances for two consecutive diurnal cycles during wet and dry seasons over rainforest and pasture sites with different annual rainfall (e.g., K34 as a wet site and FNS as a dry site, annual rainfall 2329 and 1597 mm) (Fig. 7). Our results confirm the occurrence of diurnal hysteresis between $g_C - g_A$ and λE_T and explain the reason for the shape of the curves obtained in Fig. 6. During the wet season, a distinct environmental control is detectable on g_C and λE_T in the morning hours (Fig. 7a and b) in both the PFTs where g_C and λE_T increased as a result of increasing R_N, T_R, and D_A. From the late morning to afternoon, a near-constant (forest) or negligible (pasture) increase in λE_T is observed despite substantial reduction of both g_C and g_A (25 to 50 % decrease), after which λE_T starts decreasing. This behavior of λE_T was triggered due to the concurrent

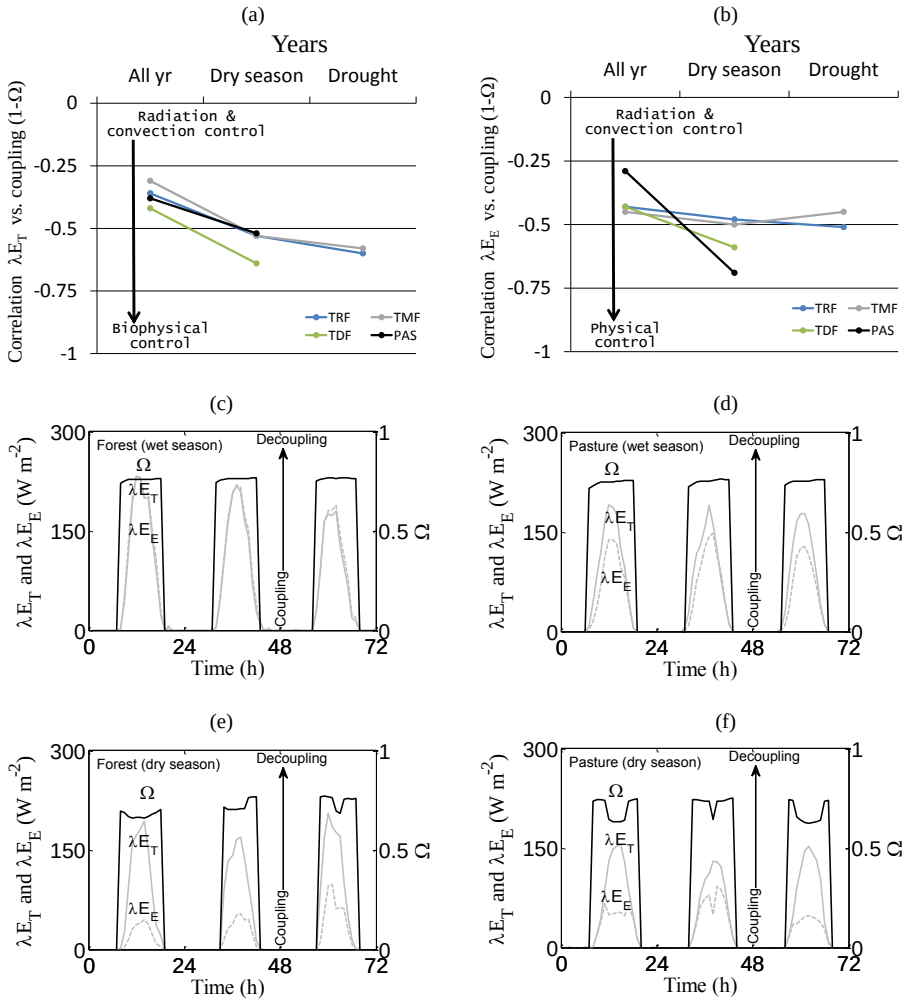

Figure 5. Correlation of coupling $(1-\Omega)$ with **(a)** transpiration (λE_T) and **(b)** evaporation (λE_E) and over four different PFTs by combining data for all the years, only during dry seasons for all the years, and during drought year 2005. Data for 2005 were not available for TDF and PAS. **(c)**–**(e)** Examples of the diurnal pattern of Ω (black lines), λE_E (grey dotted lines) and λE_T (grey solid lines) estimated over two ecohydrologically contrasting biomes (K34 for forest and FNS for pasture) in the Amazon Basin (LBA tower sites) during wet and dry seasons.

changes in R_N (15 to 50 % change), D_A (20 to 60 % change), and T_R (5 to 14 % change), which indicates the absence of any dominant biophysical regulation on λE_T during the wet season (Fig. 7a and b). On the contrary, in the dry season, although the morning rise in λE_T is steadily controlled by the integrated influence of environmental variables, a modest to strong biophysical control is found for both PFTs during the afternoon, where λE_T substantially decreased with decreasing conductances (Fig. 7c and d). This decrease in λE_T is mainly caused by the reduction in g_C as a result of increasing D_A and T_R (as seen later in Fig. 8a and c). In the dry season, the area under the hysteretic relationship between λE_T, g_C, and environmental variables was substantially wider in pasture (Fig. 7d) than for the rainforest (Fig. 7c), which is attributed to a greater hysteresis area between R_N and D_A in pasture as a result of reduced water supply. The stronger hysteresis effects in pasture during the dry season (Fig. 7d) ultimately led to the stronger relationship between coupling and λE_T (as seen in Fig. 5a).

4.4 Factors affecting variability of g_C and g_A

The sensitivity of stomatal conductance to vapor pressure deficit is a key governing factor of transpiration (Ocheltree et al., 2014; Monteith, 1995). We examined whether the feedback or feed-forward response hypothesis (Monteith, 1995; Farquhar, 1987) between g_C, D_A, and λE_T is reflected in our canopy-scale g_C retrievals. Combining data of all the PFTs, we found an exponential decline of g_C in response to increasing D_A regardless of the variations of net radiation (Fig. 8a). High g_C is consistent with high humidity and low evaporative demand. Five negatively logarithmic scatters fit

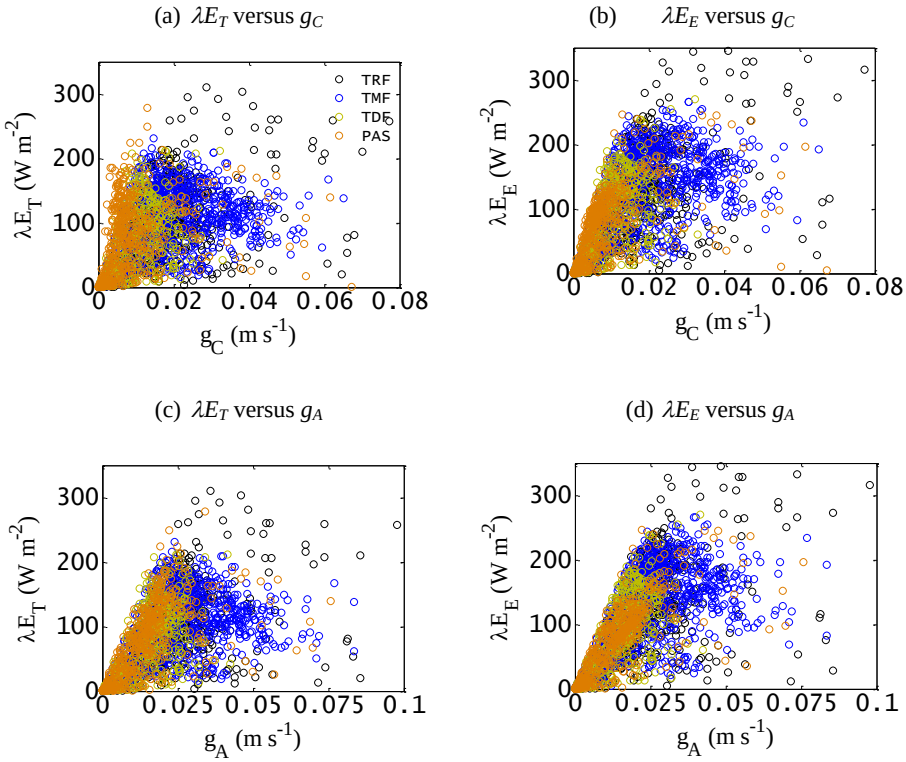

Figure 6. Scatter plots of transpiration (λE_T) and evaporation (λE_E) vs. g_C and g_A over four different PFTs in the Amazon Basin (LBA tower sites).

the data with r values of 0.38 ($0 < R_N < 150\,W\,m^{-2}$), 0.63 ($150 < R_N < 300\,W\,m^{-2}$), 0.73 ($300 < R_N < 450\,W\,m^{-2}$), 0.78 ($450 < R_N < 600\,W\,m^{-2}$), and 0.87 ($R_N > 600\,W\,m^{-2}$). The sensitivity of g_C to D_A was at the maximum in the high R_N range beyond $600\,W\,m^{-2}$ and the sensitivity progressively declined with declining magnitude of R_N (0–$150\,W\,m^{-2}$).

Scatter plots between g_C and λE_T for different levels of D_A revealed a linear pattern between them for a wide range of D_A ($20 > D_A > 0$ hPa) (Fig. 8b). Following Monteith (1995), isopleths of R_N are delineated by the solid lines passing through λE_T on the x axis and through g_C on the y axis. Isobars of D_A (dotted lines) pass through the origin because λE_T approaches zero as g_C approaches zero. Figure 8b shows substantial reduction of g_C with increasing D_A without any increase in λE_T, like an inverse hyperbolic pattern to D_A (Monteith, 1995; Jones, 1998). For all the PFTs, an active biological (i.e., stomatal) regulation maintained almost constant λE_T when D_A was changed from low to high values (Fig. 8b). At high D_A (above 10 hPa), after an initial increase in λE_T with g_C, g_C approached a maximum limit and remained nearly independent of λE_T (Fig. 8b). Among all the D_A levels, the maximum control of g_C on λE_T variability (62 to 80 %) was found at high atmospheric water demand (i.e., 30 hPa > D_A > 20 hPa). The scatter plots between g_C and T_R (Fig. 8c) for different levels of D_A revealed an exponential decline in g_C with increasing T_R and atmospheric water demand. When retrieved g_A was plotted against the radiometric surface temperature and air temperature difference ($T_R - T_A$), an exponential decline in g_A was found in response to increasing ($T_R - T_A$) (Fig. 8d). High g_A is persistent with low ($T_R - T_A$) irrespective of the variations in R_N (with the exception of very low R_N). Four negatively logarithmic scatters fit the g_A vs. ($T_R - T_A$) relationship with r values of 0.28 ($150 < R_N < 300\,W\,m^{-2}$), 0.55 ($3000 < R_N < 450\,W\,m^{-2}$), 0.64 ($450 < R_N < 600\,W\,m^{-2}$), and 0.77 ($R_N > 600\,W\,m^{-2}$).

5 Discussion

5.1 Evaluating g_A, g_C, and surface energy balance fluxes

The aerodynamic conductance retrieved with STIC1.2 showed acceptable correlation and valid estimates of g_A when compared against an empirical model that uses u^* and u to derive g_A (Figs. 1 and 2a) and two other inversion-/hybrid-based g_A estimates. The differences between $g_{A\text{-STIC}}$ and $g_{A\text{-BM13}}$ were mainly attributed to the structural differences and empirical nature of the parameterization for the near-surface boundary-layer conductance

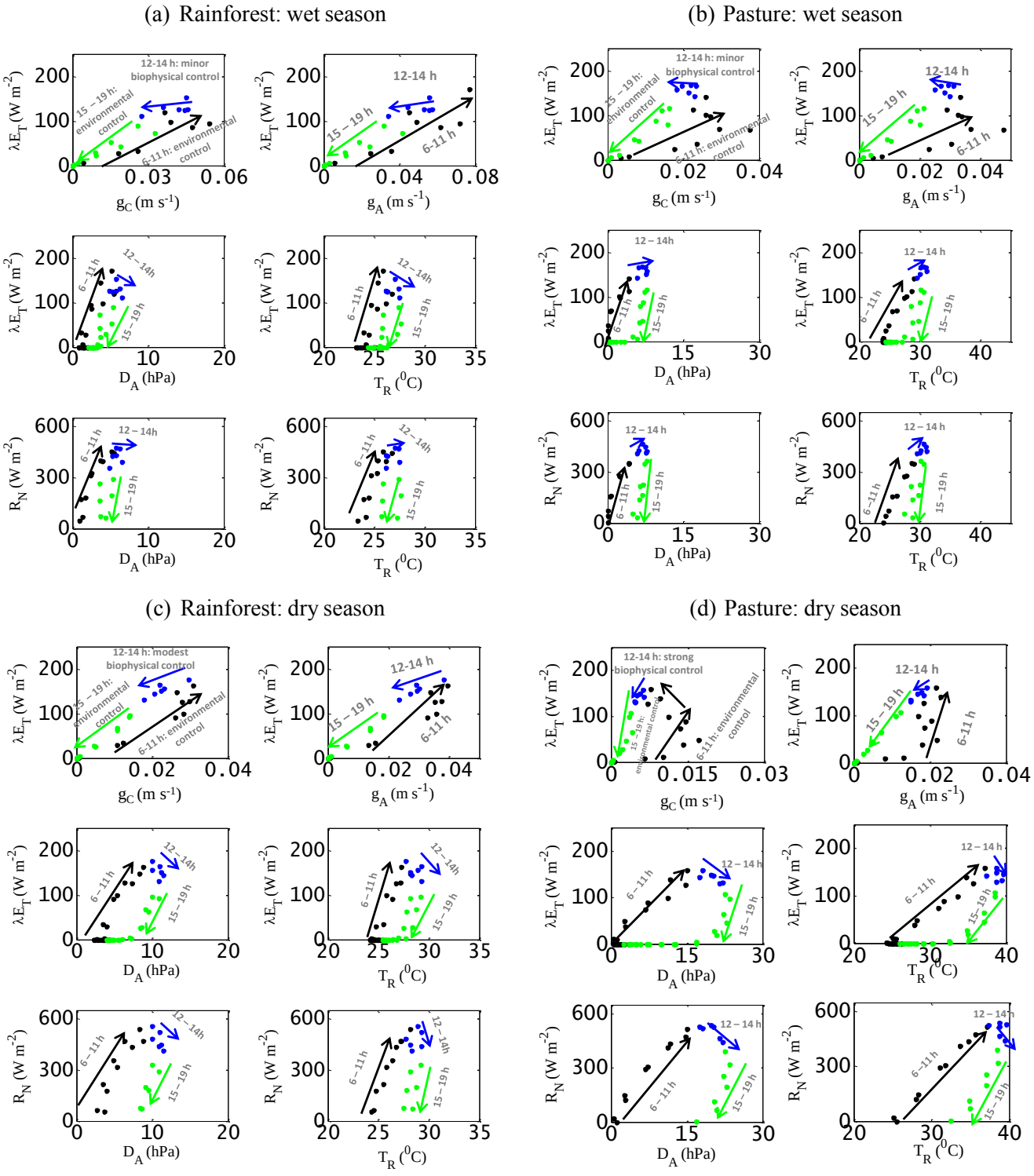

Figure 7. Illustrative examples of the occurrence of diurnal hysteresis of transpiration (λE_T) during wet and dry seasons with canopy and environmental controls over two different sites with different annual rainfall (2329 and 1597 mm, respectively) in the Amazon Basin (LBA tower sites K34 and FNS).

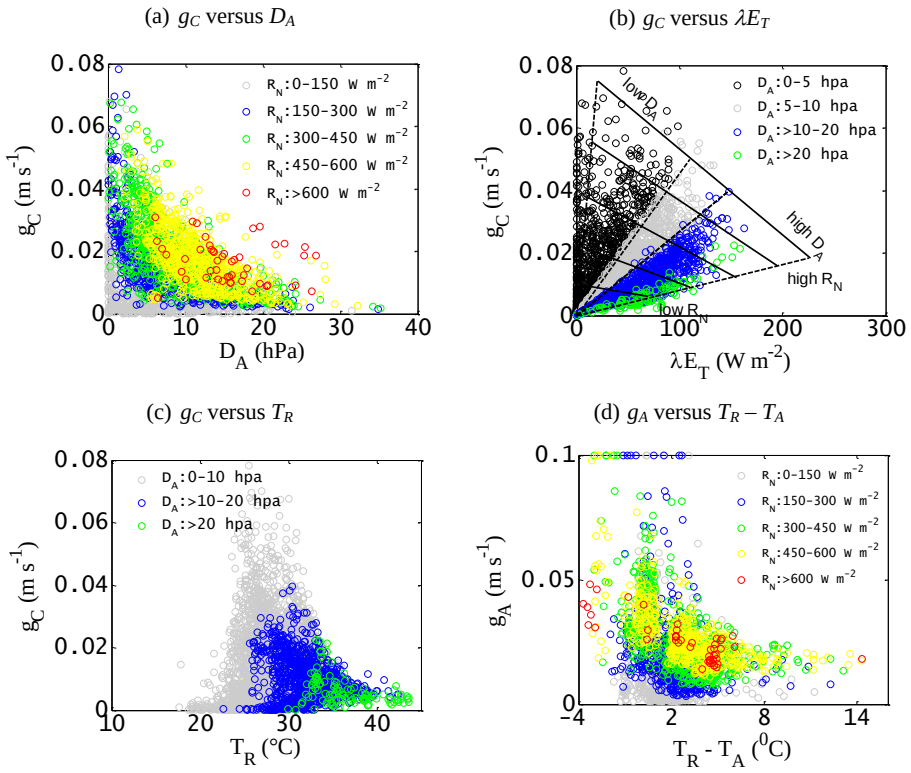

Figure 8. **(a)** Response of retrieved g_C to atmospheric vapor pressure deficit (D_A) for different classes of net radiation (R_N), **(b)** response of retrieved g_C to transpiration for different classes of D_A, **(c)** response of retrieved g_C to radiometric surface temperature (T_R) for different classes D_A, and **(d)** relationship between retrieved g_A and radiometric surface temperature and air temperature difference ($T_R - T_A$) in the Amazon Basin (LBA tower sites).

$((2/ku^{*2})(Sc/Pr)^{0.67})$ in $g_{A\text{-}BM13}$, which results in some discrepancies between $g_{A\text{-}STIC}$ and $g_{A\text{-}BM13}$, particularly in the pasture (Fig. 2a). The extent to which the structural discrepancies between $g_{A\text{-}STIC}$ and $g_{A\text{-}BM13}$ relate to actual differences in the conductances for momentum vs. heat is beyond the scope of this paper, and a detailed investigation using data on atmospheric profiles of wind speed, temperature, etc. are needed to actually quantify such differences. Momentum transfer is associated with pressure forces and is not identical to heat and mass transfer (Massman, 1999). In STIC1.2, g_A is directly estimated and is a robust representative of the conductances to heat (and water vapor) transfer, whereas $g_{A\text{-}BM13}$ estimates based on u^* and u are more representative of the momentum transfer. Therefore, the difference between the two different g_A estimates (Fig. 2) can be largely attributed to the actual difference in the conductances for momentum and heat (water vapor). The turbulent conductance equation (u^{*2}/u) in $g_{A\text{-}BM13}$ is also very sensitive to the uncertainties in the sonic anemometer measurement (Contini et al., 2006; Richiardone et al., 2012). However, the evidence of a weak systematic relationship between the g_A residuals and u (Fig. 2d) and the capability of the thermal (T_R), radiative (ϕ), and meteorological (T_A, D_A) variables in capturing the variability of $g_{A\text{-}BM13}$ (Fig. 2e and f) indicates the diagnostic potential $g_{A\text{-}STIC}$ estimates to explain the wind-driven g_A variability. Excluding u might introduce errors in cases where wind is the only source of variations in g_A and surface fluxes (Mallick et al., 2015). In general, the accuracies in commonly used parametric g_A estimates based on u and surface roughness parameters several meters distant from canopy foliage are limited due to the uncertainties concerning the attenuation of u close to the vegetation surface (Meinzer et al., 1997; Prihodko et al., 2008). The magnitude of u near the foliage can be substantially lower than that measured considerably away at some reference location above or within the canopy (Meinzer et al., 1997). Notwithstanding the inequalities of g_A estimated with different methods, it is challenging to infer the accuracy of the different estimates. It is imperative to mention that g_A is one of the main anchors in the PM–SW model because it not only appears in the numerator and denominator of these models, but also provides feedback to g_C, T_0, and D_0 (the seminal paper of Jarvis and McNaughton, 1986). Therefore, the estimates of λE in the PM–SW framework are very sensitive to parameterization of g_A and stable λE estimates might be possible if g_A estimation is unambiguous (Holwerda et al., 2012; Van Dijk et al., 2015). Given the lack of consensus in the community on the "true" g_A and from the nature of surface flux validation re-

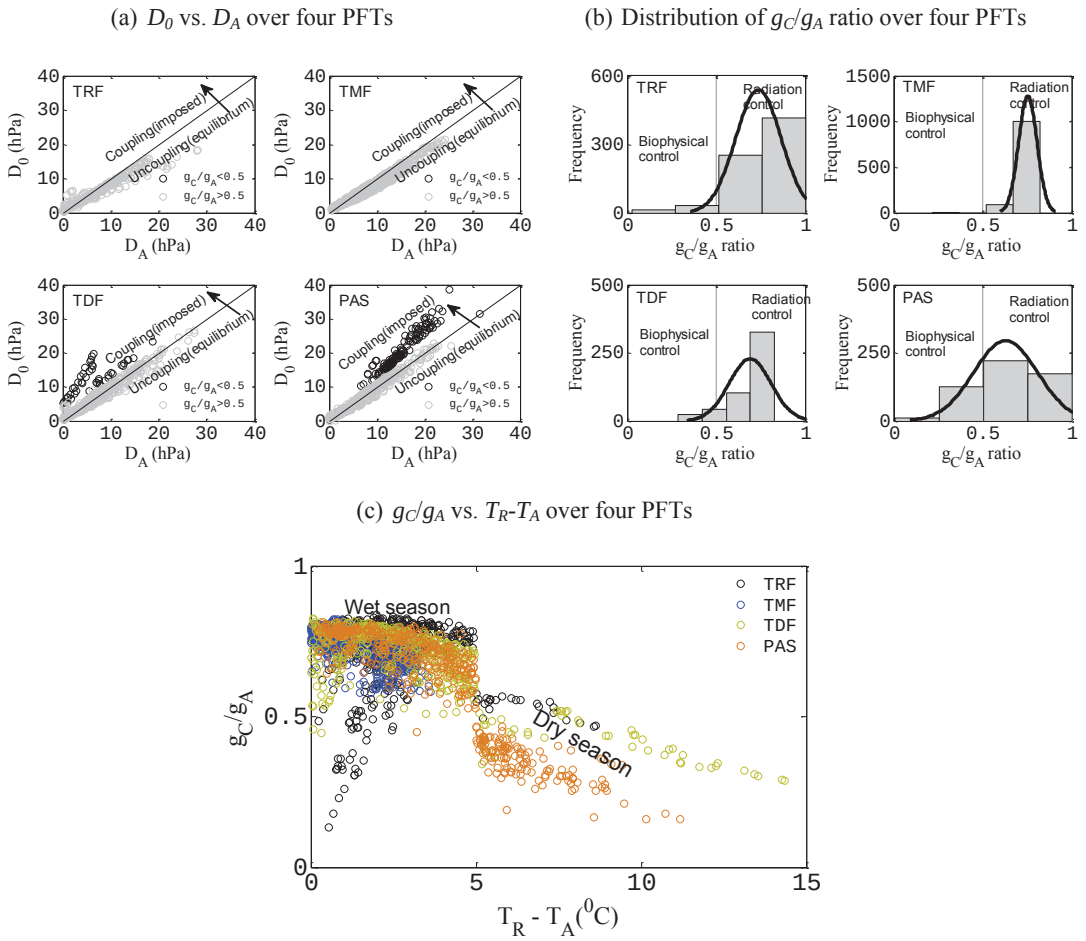

Figure 9. (a) Scatter plots between source/sink height (or in-canopy) vapor pressure deficit (D_0) and atmospheric vapor pressure deficit (D_A) for two different classes of g_C / g_A ratios over four PFTs, which clearly depicts a strong coupling between D_0 and D_A for low g_C / g_A ratios. **(b)** Histogram distribution of g_C / g_A ratios over the four PFTs in the Amazon Basin (LBA tower sites). **(c)** Scatter plots between g_C / g_A ratio vs. surface air temperature difference ($T_R - T_A$) for the four PFTs during the wet season and dry season in the Amazon Basin (LBA tower sites).

sults (Fig. 4), it appears that $g_{A\text{-STIC}}$ tends to be the appropriate aerodynamic conductance that satisfies the PM–SW equation. Discrepancies between $g_{C\text{-STIC}}$ and $g_{C\text{-INV}}$ originated from the differences in g_A estimates between the two methods.

Despite the good agreement between the measured and predicted λE and H (Fig. 4, Table 4), the larger error in H was associated with the higher sensitivity of H to the errors in T_R (due to poor emissivity correction) (Mallick et al., 2015). Since the difference between T_R and T_A is considered to be the primary driving force of H (van der Tol et al., 2009), the modeled errors in H are expected to arise due to the uncertainties associated with T_R.

5.2 Canopy coupling, g_C, and g_A vs. transpiration and evaporation

The correlation analysis between $1 - \Omega$ and λE_T revealed the extent of biophysical and radiative controls on λE_T (Fig. 5). The degree of biophysical control is a function of the ratio of g_C to g_A. Minor biophysical control on λE_T was apparent for forest and pasture during the wet seasons (Fig. 5c and d) as a result of a high g_C / g_A ratio along with increasing λE_T. Such conditions stimulate local humidification of air surrounding the canopy and uncoupling of the in-canopy vapor pressure deficit (D_0) from that in the air above (i.e., $D_0 < D_A$) (Meinzer et al., 1997; Motzer et al., 2005) (Fig. 9a), which implies that λE_T becomes largely independent of g_C. By contrast, an enhanced biophysical control on λE_T was apparent during the dry season and drought year 2005 during the period of reduced water supply, particularly over PAS (Figs. 5e, f, and 7). Such a condition leads to a relatively dry

Table 3. Comparative statistics for the STIC- and tower-derived hourly g_A and g_C for a range of PFTs in the Amazon Basin (LBA tower sites). Values in parentheses are ±1 standard deviation (standard error for correlation).

	$g_{A\text{-STIC}}$ vs. $g_{A\text{-BM13}}$				$g_{C\text{-STIC}}$ vs. $g_{C\text{-INV}}$				
PFTs	RMSD ($m\,s^{-1}$)	R^2	Slope	Offset ($m\,s^{-1}$)	RMSD ($m\,s^{-1}$)	R^2	Slope	Offset ($m\,s^{-1}$)	N
TRF	0.013	0.41 (±0.03)	1.07 (±0.047)	0.0031 (±0.0008)	0.012	0.14 (±0.04)	0.39 (±0.039)	0.0097 (±0.0007)	1159
TMF	0.012	0.55 (±0.12)	0.81 (±0.023)	0.0006 (±0.0006)	0.009	0.55 (±0.12)	0.85 (±0.025)	0.0032 (±0.0005)	1927
TDF	0.007	0.49 (±0.15)	0.89 (±0.041)	0.0019 (±0.0006)	0.012	0.33 (±0.19)	0.30 (±0.022)	0.0050 (±0.0005)	787
PAS	0.012	0.22 (±0.18)	1.03 (±0.083)	0.0059 (±0.0007)	0.007	0.58 (±0.12)	0.65 (±0.025)	0.0024 (±0.0003)	288
Mean	**0.012**	**0.44 (±0.10)**	**0.76 (±0.016)**	**0.0047 (±0.003)**	**0.010**	**0.39 (±0.08)**	**0.63 (±0.016)**	**0.0046 (±0.0003)**	**4161**

N: number of data points; RMSD: root mean square deviation between predicted (P) and observed (O) variables $= \left[\frac{1}{N}\sum_{i=0}^{N}(P_i - O_i)^2\right]^2$.

Table 4. Comparative statistics for the STIC- and tower-derived hourly λE and H for a range of PFTs in the Amazon Basin (LBA tower sites). Values in parentheses are ±1 standard deviation (standard error for correlation).

	λE				H				
PFTs	RMSD ($W\,m^{-2}$)	R^2	Slope	Offset ($W\,m^{-2}$)	RMSD ($W\,m^{-2}$)	R^2	Slope	Offset ($W\,m^{-2}$)	N
TRF	28	0.96 (±0.007)	1.10 (±0.008)	−16 (±2)	34	0.52 (±0.030)	0.60 (±0.025)	29 (±2)	1159
TMF	20	0.98 (±0.004)	1.08 (±0.004)	−11 (±1)	23	0.71 (±0.019)	0.61 (±0.014)	20 (±1)	1927
TDF	26	0.96 (±0.009)	0.96 (±0.008)	−7 (±2)	30	0.66 (±0.032)	0.89 (±0.035)	20 (±3)	787
PAS	31	0.96 (±0.009)	1.14 (±0.010)	−2 (±2)	33	0.88 (±0.016)	0.67 (±0.011)	9 (±1)	288
Mean	**33**	**0.94 (±0.005)**	**1.04 (±0.005)**	**−1 (±1)**	**37**	**0.61 (±0.021)**	**0.58 (±0.009)**	**24 (±2)**	**4161**

canopy surface and substantially high g_A compared to g_C, thus resulting in low g_C/g_A ratios regardless of their absolute values (Meinzer et al., 1993; McNaughton and Jarvis, 1991). Here, a fractional change in g_C results in an equivalent fractional change in λE_T. This impedes transpiration from promoting local equilibrium of D_0 and minimizing (or maximizing) the gradient between D_0 and atmospheric vapor pressure deficit (D_A) (i.e., $D_0 \cong D_A$ or $D_0 > D_A$) (Eq. A10) (Fig. 9a), thereby resulting in strong coupling between D_0 and D_A (Meinzer et al., 1993; Jarvis and McNaughton, 1986). Besides, a supplemental biophysical control on λE_T might have been imposed as a consequence of a direct negative feedback of D_A and D_0 on g_C (McNaughton and Jarvis, 1991; Jarvis, 1986). An increase in D_A (or D_0) beyond a certain limit decreases g_C (Figs. 7 and 8), resulting in a low and narrow increase in λE_T, despite a steady increase in g_A and R_N. The combination of a negative feedback response between D_A and g_C with the overall radiative–aerodynamic coupling significantly dampens the variation of transpiration in PAS and TDF in the dry season, thus featuring increased biophysical control in these PFTs. These results are in agreement with von Randow et al. (2012), who found enhanced biophysical control on λE_T for the pasture during the dry season. For the wet season, evidence of minor biophysical control indicates

the dominance of R_N-driven equilibrium evaporation in these PFTs (Hasler and Avissar, 2007; da Rocha et al., 2009; Costa et al., 2010). In the TRF and TMF, 94 and 99 % of the retrieved g_C / g_A ratios fall above 0.5, and only 1 and 6 % of the retrieved g_C / g_A ratios fall below the 0.5 range (Fig. 9b). In contrast, 90 and 73 % of the g_C / g_A ratios range above 0.5, and 10 to 27 % of the g_C / g_A ratios were below 0.5 for TDF and PAS, respectively (Fig. 9b). This shows that, although radiation control is prevailing in all the sites, biophysical control is relatively stronger in TDF and PAS as compared to the other sites. For large g_C / g_A ratios, the conditions within the planetary boundary layer (PBL) become decoupled from the synoptic scale (McNaughton and Jarvis, 1991) and the net radiative energy becomes the important regulator of transpiration. For small g_C / g_A ratios (e.g., in the dry season), the conditions within the PBL are strongly coupled to the atmosphere above by rapid entrainment of air from the capping inversion and by some ancillary effects of sensible heat flux on the entrainment (McNaughton and Jarvis, 1991). These findings substantiate the earlier theory of McNaughton and Jarvis (1991), who postulated that large g_C / g_A ratios result in minor biophysical control on canopy transpiration due to the negative feedback on the canopy from the PBL. The negative relationship between $1 - \Omega$ and λE_E (Fig. 5b) over all the PFTs is due to the feedback of g_A on g_C. However, over all the PFTs, a combined control of g_A and environmental variables on λE_E again highlighted the impact of realistically estimated g_A on λE_E (Holwerda et al., 2012).

It is important to mention that forests are generally expected to be better coupled to the atmosphere as compared to the pastures, which is related to generally higher g_A of the forests (due to high surface roughness). This implies that forests exhibit stronger biophysical control on λE_T. However, due to the broad leaves of the rainforests (larger leaf area index) and higher surface wetness (due to higher rainfall amounts), the wet surface area is much larger in the forests than in the pastures. This results in much higher g_C values for forests than for pastures during the wet season ($g_C \approx g_A$), and $g_C / g_A \to 1$. Consequently, no significant difference in coupling was found between them during the wet season (Fig. 5c and d). Despite the absolute differences in g_A and g_C between forest and pasture, the high surface wetness is largely offsetting the expected Ω difference between them. Although the surface wetness is substantially lower during the dry season, the high water availability in the forests due to the deeper root systems helps in maintaining a relatively high g_C compared to the pastures. Hence, despite g_A (forest) > g_A (pasture) during the dry season, substantially lower g_C values for the pasture result in a lower g_C / g_A ratio for the pasture compared to the forest, thus causing more biophysical control on λE_T during the dry season. The relatively better relationship between coupling vs. λE_T in PAS and TDF during the dry season was also attributed to high surface air temperature differences ($T_R - T_A$) in these PFTs that resulted in low g_C / g_A ratios (Fig. 9c).

5.3 Factors affecting g_C and g_A variability

The stomatal feedback-response hypothesis (Monteith, 1995) also became apparent at the canopy scale (Fig. 8a and b), which states that a decrease in g_C with increasing D_A is caused by a direct increase in λE_T (Monteith, 1995; Matzner and Comstock, 2001; Streck, 2003), and g_C responds to the changes in the air humidity by sensing λE_T rather than D_A. This feedback mechanism is found because of the influence of D_A on both g_C and λE_T, which in turn changes D_A by influencing the air humidity (Monteith, 1995). The change in g_C is dominated by an increase in the net available energy, which is partially offset by an increase in λE_T. After the net energy input in the canopy exceeds a certain threshold, g_C starts decreasing even if λE_T increases. High λE_T increases the water potential gradient between guard cells and other epidermal cells or reduces the bulk leaf water potential, thus causing stomatal closure (Monteith, 1995; Jones, 1998; Streck, 2003). The control of soil water on transpiration also became evident from the scatter plots between g_C vs. λE_T and T_R for different D_A levels (Figs. 8b, c, and 7). Denmead and Shaw (1962) hypothesized that reduced g_C and stomatal closure occurs at moderate to higher levels of soil moisture (high λE_T) when the atmospheric demand of water vapor increases (high D_A). The water content in the immediate vicinity of the plant root depletes rapidly at high D_A, which decreases the hydraulic conductivity of soil, and the soil is unable to efficiently supply water under these conditions. For a given evaporative demand and available energy, transpiration is determined by the g_C / g_A ratio, which is further modulated by the soil water availability. These combined effects tend to strengthen the biophysical control on transpiration (Leuzinger and Kirner, 2010; Migletta et al., 2011). The complex interaction between g_C, T_R, and D_A (Fig. 8c) explains why different parametric g_C models produce divergent results.

Although λE_T and λE_E estimates are interdependent on g_C and g_A (as shown in Figs. 6–8), the figures reflect the credibility of the conductances as well as transpiration estimates by realistically capturing the hysteretic behavior between biophysical conductances and water vapor fluxes, which is frequently observed in natural ecosystems (Zhang et al., 2014; Renner et al., 2016) (also Zuecco et al., 2016). These results are also compliant with the theories postulated earlier from observations that the magnitude of hysteresis depends on the radiation–vapor pressure deficit time lag, while the soil moisture availability is a key factor modulating the hysteretic transpiration–vapor pressure deficit relation as soil moisture declines (Zhang et al., 2014; O'Grady et al., 1999; Jarvis and McNaughton, 1986). This shows that despite being independent of any predefined hysteretic function, the interdependent conductance–transpiration hysteresis is still captured in STIC1.2.

Figure 8d is in accordance with the existing theory that under conditions of extremely high atmospheric turbulence

(i.e., high g_A), a close coupling exists between the surface and the atmosphere, which causes T_R and T_A to converge (i.e., $T_R - T_A \to 0$). When g_A is low, the difference between T_R and T_A increases due to poor vertical mixing of the air.

6 Conclusions

By integrating the radiometric surface temperature (T_R) into a combined structure of the PM–SW model, we have estimated the canopy-scale biophysical conductances and quantified their control on the terrestrial evapotranspiration components in a simplified SEB modeling perspective that treats the vegetation canopy as "big-leaf". The STIC1.2 biophysical modeling scheme is independent of any leaf-scale empirical parameterization for stomata and associated aerodynamic variables.

Stomata regulate the coupling between terrestrial carbon and water cycles, which implies that their behavior under global environmental change is critical to predicting vegetation functioning (Medlyn et al., 2011). The combination of variability in precipitation (Hilker et al., 2014) and land cover change (Davidson et al., 2012) in the Amazon Basin is expected to increase the canopy–atmosphere coupling of pasture or forest systems under drier conditions by altering the ratio of the biological and aerodynamic conductances. An increase in biophysical control will most likely be an indicator of shifting the transpiration from an energy-limited to a water-limited regime (due to the impact of T_R, T_A, and D_A on the g_C / g_A ratio), with further consequences for the surface water balance and rainfall recycling. At the same time, a transition from forest to pasture or agriculture lands will substantially reduce the contribution of interception evaporation in the Amazon; hence, it will affect the regional water cycle. This might change the moisture regime of the Amazonian Basin and affect the moisture transport to other regions. In this context, STIC1.2 provides a new quantitative and internally consistent method for interpreting the biophysical conductances and is able to quantify their controls on the water cycle components in response to a range of climatic and eco-hydrological conditions (excluding rising atmospheric CO_2) across a broad spectrum of PFTs. It could also provide the basis for improving existing land surface parameterizations for simulating vegetation water use at large spatial scales.

It should also be noted that although the case study described here provides general insights into the biophysical controls of λE and associated feedback between g_C, D_A, T_R, and λE_T in the framework of the PM–SW equation, there is a tendency to overestimation of g_C due to the embedded evaporation information in the current single-source composition of STIC1.2. For accurate characterization of canopy conductance, explicit partitioning of λE into transpiration and evaporation (both soil and interception) is one of the further scopes for improving STIC1.2, and this assumption needs to be tested further.

7 Data availability

The LBA eddy covariance datasets are available through ftp://daac.ornl.gov/data/lba/carbon_dynamics/CD32_Brazil_Flux_Network/ (Saleska et al., 2013).

Appendix A: Description of STIC1.2

A1 Derivation of "state equations" in STIC 1.2

Neglecting horizontal advection and energy storage, the surface energy balance equation is written as follows:

$$\phi = \lambda E + H. \tag{A1}$$

Figure A1 shows that, while H is controlled by a single aerodynamic resistance (r_A) (or $1/g_A$); λE is controlled by two resistances in series, the surface resistance (r_C) (or $1/g_C$) and the aerodynamic resistance to vapor transfer ($r_C + r_A$). For simplicity, it is implicitly assumed that the aerodynamic resistance of water vapor and heat are equal (Raupach, 1998), and both the fluxes are transported from the same level from near surface to the atmosphere. The sensible and latent heat flux can be expressed in the form of aerodynamic transfer equations (Boegh et al., 2002; Boegh and Soegaard, 2004) as follows:

$$H = \rho\, c_P\, g_A\, (T_0 - T_A) \tag{A2}$$

$$\lambda E = \frac{\rho\, c_P}{\gamma} g_A\, (e_0 - e_A) = \frac{\rho\, c_P}{\gamma} g_C \left(e_0^* - e_0\right) \tag{A3}$$

where T_0 and e_0 are the air temperature and vapor pressure at the source/sink height (i.e., aerodynamic temperature and vapor pressure) or at the so-called roughness length (z_0), where wind speed is zero. They represent the vapor pressure and temperature of the quasi-laminar boundary layer in the immediate vicinity of the surface level (Fig. A1), and T_0 can be obtained by extrapolating the logarithmic profile of T_A down to z_0. e_0^* is the saturation vapor pressure at T_0 (hPa).

By combining Eqs. (A1)–(A3) and solving for g_A, we get the following equation.

$$g_A = \frac{\phi}{\rho c_P}\left[(T_0 - T_A) + \left(\frac{e_0 - e_A}{\gamma}\right)\right] \tag{A4}$$

Combining the aerodynamic expressions of λE in Eq. (A3) and solving for g_C, we can express g_C in terms of g_A, e_0^*, e_0, and e_A.

$$g_C = g_A \frac{(e_0 - e_A)}{\left(e_0^* - e_0\right)} \tag{A5}$$

While deriving the expressions for g_A and g_C, two more unknown variables are introduced (e_0 and T_0), thus there are two equations and four unknowns. Therefore, two more equations are needed to close the system of equations.

An expression for T_0 is derived from the Bowen ratio (β) (Bowen, 1926) and evaporative fraction (Λ) (Shuttleworth et al., 1989) equation.

$$\beta = \left(\frac{1-\Lambda}{\Lambda}\right) = \frac{\gamma\,(T_0 - T_A)}{(e_0 - e_A)} \tag{A6}$$

$$T_0 = T_A + \left(\frac{e_0 - e_A}{\gamma}\right)\left(\frac{1-\Lambda}{\Lambda}\right) \tag{A7}$$

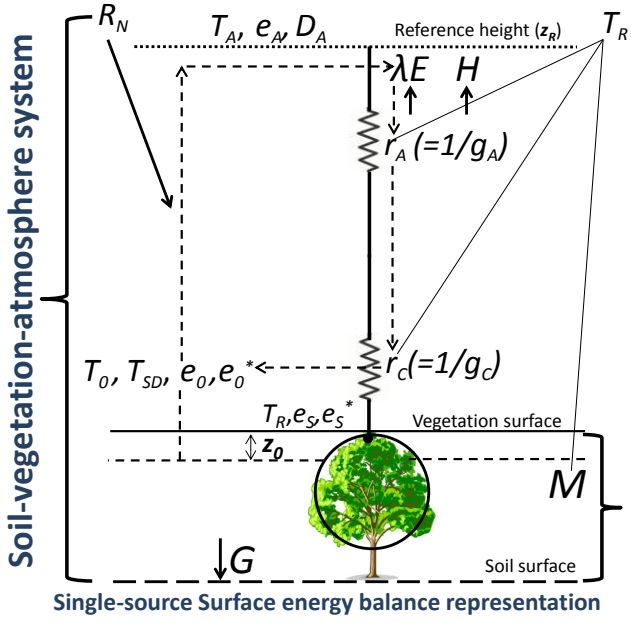

Figure A1. Schematic representation of the one-dimensional description of STIC1.2. In STIC1.2, a feedback is established between the surface-layer evaporative fluxes and source/sink height mixing and coupling, and the connection is shown in dotted arrows between e_0, e_0^*, g_A, g_C, and λE. Here, r_A and r_C are the aerodynamic and canopy (or surface in the case of partial vegetation cover) resistances, g_A and g_C are the aerodynamic and canopy conductances (reciprocal of resistances), e_S^* is the saturation vapor pressure of the surface, e_0^* is the saturation vapor pressure at the source/sink height, T_0 is the source/sink height temperature (i.e., aerodynamic temperature) that is responsible for transferring the sensible heat (H), e_0 is the source/sink height vapor pressure, e_S is the vapor pressure at the surface, z_0 is the roughness length, T_R is the radiometric surface temperature, T_{SD} is the source/sink height dew-point temperature, M is the surface moisture availability or evaporation coefficient, R_N and G are net radiation and ground heat flux, T_A, e_A, and D_A are temperature, vapor pressure, and vapor pressure deficit at the reference height (z_R), λE is the latent heat flux, and H is the sensible heat flux, respectively.

This expression for T_0 introduces another new variable (Λ); therefore, one more equation that describes the dependence of Λ on the conductances (g_A and g_C) is needed to close the system of equations. In order to express Λ in terms of g_A and g_C, we had adopted the advection–aridity (AA) hypothesis (Brutsaert and Stricker, 1979) with a modification introduced by Mallick et al. (2015). The AA hypothesis is based on a complementary connection between the potential evaporation (E^*), sensible heat flux (H), and E; and leads to an assumed link between g_A and T_0. However, the effects of surface moisture (or water stress) were not explicit in the AA equation, and Mallick et al. (2015) implemented a moisture constraint in the original AA hypothesis while deriving a "state equation" of Λ (Eq. A8 below). A detailed derivation of the "state equation" for Λ is described in Supplement S1

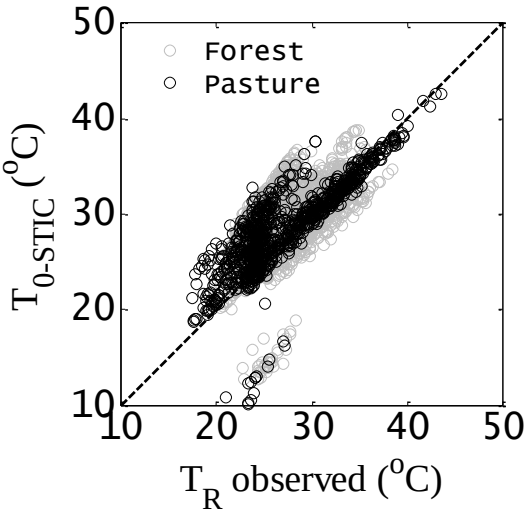

Figure A2. Aerodynamic temperature obtained from STIC1.2 ($T_{0\text{-STIC}}$) vs. radiometric surface temperature (T_R) over two different biomes in the Amazon Basin. The regression equation of line of best fit is $T_{0\text{-STIC}} = 0.67\ (\pm 0.10)\ T_R + 10.59\ (\pm 2.79)$ with $r = 0.65$.

(also see Mallick et al., 2014, 2015). Estimation of e_0, e_0^*, M, and α is described in Appendix A2.

$$\Lambda = \frac{2\alpha s}{2s + 2\gamma + \gamma \frac{g_A}{g_C}(1+M)} \tag{A8}$$

A2 Iterative solution of e_0, e_0^*, M, and α in STIC 1.2

In STIC1.0 and 1.1 (Mallick et al., 2014, 2015), no distinction was made between the surface and source/sink height vapor pressures. Therefore, e_0^* was approximated as the saturation vapor pressure at T_R and e_0 was empirically estimated from M based on the assumption that the vapor pressure at the source/sink height ranges between extreme wet–dry surface conditions. However, the level of e_0 and e_0^* should be consistent with the level of the aerodynamic temperature (T_0) from which the sensible heat flux is transferred (Lhomme and Montes, 2014). The predictive use of the PM model could be hindered by neglecting of the feedbacks between the surface-layer evaporative fluxes and source/sink height mixing and coupling (McNaughton and Jarvis, 1984) and their impact on the canopy-scale conductances. Therefore, in STIC1.2, we have used physical expressions for estimating e_0 and e_0^* followed by estimating T_{SD} and M as described below. The fundamental differences between the STIC1.0, 1.1, and 1.2 modeling philosophies are described in Table A1.

An estimate of e_0^* is obtained by inverting the aerodynamic transfer equation of λE.

$$e_0^* = e_A + \left[\frac{\gamma \lambda E\,(g_A + g_C)}{\rho c_P g_A g_C}\right] \tag{A9}$$

Following Shuttleworth and Wallace (1985) (SW), the vapor pressure deficit (D_0) ($= e_0^* - e_0$) and vapor pressure (e_0) at the source/sink height are expressed as follows.

$$D_0 = D_A + \left[\frac{\{s\phi - (s+\gamma)\lambda E\}}{\rho c_P g_A}\right] \tag{A10}$$

$$e_0 = e_0^* - D_0 \tag{A11}$$

A physical equation of α is derived by expressing the evaporative fraction (Λ) as a function of the aerodynamic equations of H [$\rho c_P\, g_A (T_0 - T_A)$] and λE [$\frac{\rho c_P}{\gamma}\, \frac{g_A g_C}{g_A + g_C}(e_0^* - e_A)$] as follows.

$$\Lambda = \frac{\lambda E}{H + \lambda E} \tag{A12}$$

$$= \frac{\frac{\rho c_P}{\gamma}\, \frac{g_A g_C}{g_A + g_C}\left(e_0^* - e_A\right)}{\rho c_P g_A\,(T_0 - T_A) + \frac{\rho c_P}{\gamma}\, \frac{g_A g_C}{g_A + g_C}\left(e_0^* - e_A\right)} \tag{A13}$$

$$= \frac{g_C\left(e_0^* - e_A\right)}{\left[\gamma\,(T_0 - T_A)\,(g_A + g_C) + g_C\left(e_0^* - e_A\right)\right]} \tag{A14}$$

Combining Eqs. (A14) and (A8) (eliminating Λ), we can derive a physical equation of α.

$$\alpha = \frac{g_C\left(e_0^* - e_A\right)\left[2s + 2\gamma + \gamma \frac{g_A}{g_C}(1+M)\right]}{2s\left[\gamma\,(T_0 - T_A)\,(g_A + g_C) + g_C\left(e_0^* - e_A\right)\right]} \tag{A15}$$

Following Venturini et al. (2008), M can be expressed as the ratio of the vapor pressure difference to the vapor press deficit between the surface and atmosphere as follows.

$$M = \frac{(e_0 - e_A)}{\left(e_0^* - e_A\right)} = \frac{(e_0 - e_A)}{k\left(e_S^* - e_A\right)} = \frac{s_1\,(T_{SD} - T_D)}{k s_2\,(T_R - T_D)}, \tag{A16}$$

where T_{SD} is the dew-point temperature at source/sink height and T_D is the air dew-point temperature; s_1 and s_2 are the psychrometric slopes of the saturation vapor pressure and temperature between the $(T_{SD} - T_D)$ vs. $(e_0 - e_A)$ and $(T_R - T_D)$ vs. $(e_S^* - e_A)$ relationship (Venturini et al., 2008), and k is the ratio between $(e_0^* - e_A)$ and $(e_S^* - e_A)$. Despite T_0 driving the sensible heat flux, the comprehensive dry–wet signature of the underlying surface due to soil moisture variations is directly reflected in T_R (Kustas and Anderson, 2009). Therefore, using T_R in the denominator of Eq. (A16) tends to give a direct signature of the surface moisture availability (M). In Eq. (A16), T_{SD} computation is challenging because both e_0 and s_1 are unknown. By decomposing the aerodynamic equation of λE, T_{SD} can be expressed as follows.

$$\lambda E = \frac{\rho c_P}{\gamma} g_A\,(e_0 - e_A) = \frac{\rho c_P}{\gamma} g_A s_1\,(T_{SD} - T_D) \tag{A17}$$

$$T_{SD} = T_D + \frac{\gamma \lambda E}{\rho c_P g_A s_1} \tag{A18}$$

In the earlier STIC versions, s_1 was approximated at T_D, e_0^* was approximated at T_R, T_{SD} was estimated from s_1, T_D, T_R, and related saturation vapor pressures (Mallick et al., 2014, 2015), and M was estimated from Eq. (A16) (estimation of T_{SD} and M was stand-alone earlier). However, since

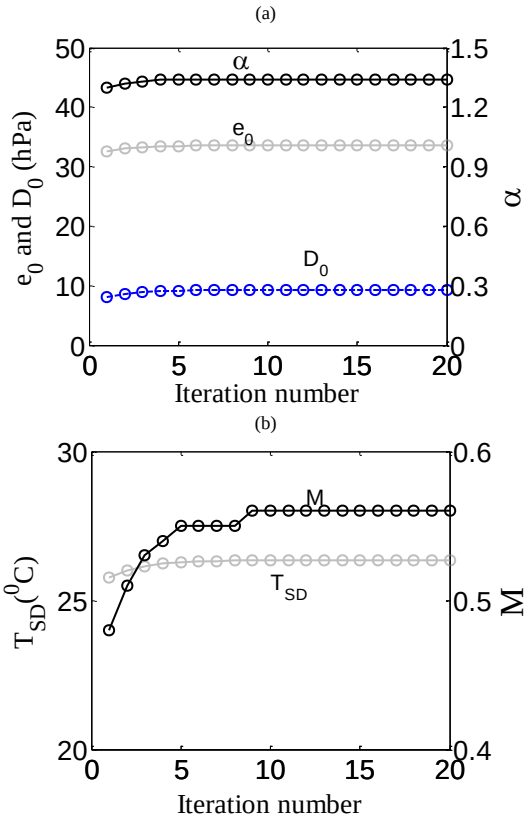

Figure A3. (a) Convergence of the iteration method for retrieving the source/sink height (or in-canopy) vapor pressures (e_0 and D_0) and Priestley–Taylor coefficient (α). **(b)** Convergence of the iteration method for retrieving the surface wetness (M) and source/sink height dew-point temperature (T_{SD}). The initial values of λE, g_A, g_C, and T_0 were determined with $\alpha = 1.26$. The process is then iterated by updating λE, e_0, D_0, M, T_{SD}, and α in subsequent iterations with the previous estimates of g_A, g_C, and T_0.

T_{SD} depends on λE and g_A, an iterative procedure is applied to estimate T_{SD} and M as described in the following paragraph.

In STIC1.2, an initial value of α is assigned as 1.26 and initial estimates of e_0^* and e_0 are obtained from T_R and M as $e_0^* = 6.13753e^{\frac{17.27T_R}{(T_R+237.3)}}$ and $e_0 = e_A + M(e_0^* - e_A)$. Initial T_{SD} and M were estimated as described in Mallick et al. (2014, 2015). With the initial estimates of these variables, first estimates of the conductances, T_0, Λ, and λE are obtained. The process is then iterated by updating e_0^* (using Eq. A9), D_0 (using Eq. A10), e_0 (using Eq. A11), T_{SD} (using Eq. A17 with s_1 estimated at T_D), M (using Eq. A16), and α (using Eq. A15), with the first estimates of g_C, g_A, and λE, and recomputing g_C, g_A, T_0, Λ, and λE in the subsequent iterations with the previous estimates of e_0^*, e_0, M, and α until the convergence of λE is achieved. Stable values of λE, e_0^*, e_0, T_{SD}, M, and α are obtained within ~ 25 iterations. Illustrative examples of the convergence of e_0^*, e_0, T_{SD}, M, and α are shown in Fig. A3.

To summarize, the computational steps of the conductances and evaporative fluxes in STIC are

- Step 1: analytical solution of the conductances, T_0 and Λ, by solving the "state equations" (Eqs. 2–5);
- Step 2: initial estimates of the conductances (g_C and g_A), T_0, Λ, λE, and H;
- Step 3: simultaneous iteration of λE, e_0^*, e_0, T_{SD}, M, and α, and final estimation of the conductances (g_C and g_A), T_0, Λ, λE, and H; and
- Step 4: partitioning λE into λE_T and λE_E.

Table A1. Differences in the modeling philosophies of source/sink height vapor pressures (e_0, e_0^*) and dew-point temperature (T_{SD}), surface wetness (M), and α between STIC1.0, STIC1.1, and STIC1.2.

Variable estimation	Principles		
	STIC1.0 (Mallick et al., 2014)	STIC1.1 (Mallick et al., 2015)	STIC1.2 (this study – Mallick et al., 2016)
Saturation vapor pressure at source/sink height (e_0^*)	e_0^* was approximated as the saturation vapor pressure at T_R.	Same as STIC1.0	e_0^* is estimated through numerical iteration by inverting the aerodynamic equation of λE (as described in Appendix A2). $e_0^* = e_A + \left[\frac{\gamma\lambda E(g_A+g_C)}{\rho c_P g_A g_C}\right]$
Actual vapor pressure at source/sink height (e_0)	e_0 was empirically estimated from M based on the assumption that the vapor pressure at the source/sink height ranges between extreme wet–dry surface conditions.	Same as STIC1.0	e_0 is estimated as $e_0 = e_0^* - D_0$, where D_0 was iteratively estimated by combining PM with the Shuttleworth–Wallace approximation (as described in Appendix A2). $D_0 = D_A + \left[\frac{\{s\phi-(s+\gamma)\lambda E\}}{\rho c_P g_A}\right]$
Dew-point temperature at source/sink height (T_{SD})	$T_{SD} = \frac{(e_S^*-e_A)-s_3T_R+s_1T_D}{(s_1-s_3)}$ s_1 and s_3 are the slopes of saturation vapor pressures at temperatures, approximated at T_D and T_R, respectively.	Same as STIC1.0	T_{SD} is estimated through numerical iteration by inverting the aerodynamic equation of λE (as described in Appendix A2). $T_{SD} = T_D + \frac{\gamma\lambda E}{\rho c_P g_A s_1}$
Surface moisture availability (M)	As a stand-alone equation, without any feedback to λE.	Same as STIC1.0	A feedback of M into λE is introduced and M is iteratively estimated after estimating T_{SD} (as described in Appendix A2).
Priestley–Taylor parameter (α)	As fixed parameter (1.26).	A physical equation of α is derived as a function of the conductances and α is numerically estimated as a variable.	A physical equation of α is derived as a function of the conductances and α is numerically estimated as a variable (Eq. A15) (as described in Appendix A2).

Table A2. Fundamental differences in the modeling principles between STIC1.2 and previous approaches for characterizing the biophysical controls on λE components.

Biophysical states	Modeling principles	
	Parametric modeling (Ma et al., 2015; Chen et al., 2011; Kumagai et al., 2004)	STIC1.2
g_A	Either g_A is assumed to be the momentum conductance (g_M) or estimated as a sum of g_M and quasi-laminar boundary-layer conductance (g_B). $1/g_A = 1/g_M + 1/g_B$ $g_M = (u^*)^2/u$ $g_B = f$ {Nusselt number, leaf dimension, thermal conductivity of air in the boundary layer, u, kinematic viscosity, Reynolds number} If u^* is available from EC tower, it is directly used, otherwise u^* is parametrized using Monin–Obukhov Similarity Theory (MOST). Disadvantages: (1) MOST is only valid for an extended, uniform, and flat surface (Foken, 2006). MOST tends to fail over rough surfaces due to breakdown of the similarity relationships for heat and water vapor transfer in the roughness sub-layer, which results in an underestimation of the "true" g_A by a factor of 1–3 (Thom et al., 1975; Chen and Schwerdtfeger, 1989; Simpson et al., 1998; Holwerda et al., 2012). (2) In the state-of-the-art λE modeling, the parametric g_A sub-models are stand-alone and empirical, and do not provide any feedback to g_C, aerodynamic temperature (T_0), and aerodynamic vapor pressures (e_0 and D_0). (3) Additional challenges in grid-scale or spatial-scale g_A estimation are the requirements of numerous site-specific parameters (e.g., vegetation height, measurement height, vegetation roughness, leaf size, soil roughness), and coefficients needed to correct the atmospheric stability conditions (Raupach, 1998).	Analytically retrieved by solving "n" state equations and "n" unknowns, with explicit convective feedback and without any wind speed (u) information. In a hallmark paper by Choudhury and Monteith (1986), it is clearly stated that "aerodynamic conductance determined by wind speed and roughness is assumed to be unaffected by buoyancy. Strictly, the aerodynamic conductance should be replaced by a term that accounts for radiative as well as convective heat transfer". The role of g_A is associated with the role of convection (Choudhury and Monteith, 1986) according to the surface energy balance principle as reflected in the derivation of Eq. (A4). Wind is generated as a result of the differences in atmospheric pressure that is a result of uneven surface radiative heating. Therefore, the aerodynamic conductance (and wind as well) is an effect of net radiative heating and there should be a physical relationship between these two. Advantages: (1) STIC1.2 consists of a feedback describing the relationship between T_R and λE, coupled with canopy–atmosphere components relating λE to T_0 and e_0. (2) Supports the findings of Villani et al. (2003) which stated that during unstable surface-layer conditions the major source of net available energy is located at the canopy top and drives the convective motion in the layers above.
g_C	(a) If λE measurements are available from the EC towers, g_C is estimated by inverting the PM equation. None of these approaches allow independent quantification of biophysical controls of λE as g_C is constrained by λE itself. (b) Sometimes g_C is modeled either by coupled leaf-scale photosynthesis models (Ball et al., 1987; Leuning, 1995) or g_C is estimated from stand-alone empirical models (Jarvis, 1976)	Analytically retrieved by solving "n" state equations and "n" unknowns where physical feedbacks of g_A, soil moisture, and vapor pressure deficit are embedded (as explained in STIC1.2 equations in the Appendix).

The Supplement related to this article is available online at doi:10.5194/hess-20-4237-2016-supplement.

Acknowledgements. This study was funded by the Luxembourg Institute of Science and Technology (LIST). The developed modeling framework contributes to the Catchments As Organized Systems (CAOS) Phase-2 research group (FOR 1598) funded by the German Science Foundation (DFG) and to the HiWET (High-resolution modelling and monitoring of Water and Energy Transfers in wetland ecosystems) consortium funded by BELSPO and FNR. We sincerely thank Andrew Jarvis (Lancaster University, UK), Monica Garcia (Technical University of Denmark, Denmark), and Georg Wohlfahrt (University of Innsbruck, Austria) for very helpful discussions and edits of the manuscript. We are grateful to all Brazilian and international collaborators and all the funding agencies that have contributed to the Large-scale Biosphere Atmosphere Experiment in Amazônia (LBA). The authors are indebted to Pavel Kabat, Antônio Ocimar Manzi, David R. Fitzjarrald, Julio Tota, Humberto Ribeiro da Rocha, Michael Goulden, Maarten J. Waterloo, and Luiz Martinelli for planning, coordinating, conducting, and evaluating the eddy covariance, meteorological, and leaf–gas exchange measurements at the LBA sites. We are particularly grateful to all field technicians whose hard work was the key ingredient to establishing the quality of the datasets used in this paper. The authors declare no conflict of interest. Darren T. Drewry acknowledges the support of the Jet Propulsion Laboratory, California Institute of Technology, under a contract with the National Aeronautics and Space Administration.

Edited by: P. Saco
Reviewed by: four anonymous referees

References

Anderson, M. C., Norman, J. M., Kustas, W. P., Li, F., Prueger, J. H., and Mecikalski, J. R.: A climatological study of evapotranspiration and moisture stress across the continental United States: 1. Model formulation, J. Geophys. Res., 112, D11112, doi:10.1029/2006JD007507, 2007.

Andreae, M. O., Artaxo, P., Brandao, C., Carswell, F. E., Ciccioli, P., da Costa, A. L., Culf, A. D., Esteves, J. L., Gash, J. H. C., Grace, J., Kabat, P., Lelieveld, J., Malhi, Y., Manzi, A. O., Meixner, F. X., Nobre, A. D., Nobre, C., Ruivo, M. d. L. P., Silva-Dias, M. A., Stefani, P., Valentini, R., von Jouanne, J., and Waterloo, M. J.: Biogeochemical cycling of carbon, water, energy, trace gases, and aerosols in Amazonia: The LBA-EUSTACH experiments, J. Geophys. Res., 107, D208066, doi:10.1029/2001JD000524, 2002.

Baker, I. T., Harper, A. B., da Rocha, H. R., Denning, A. S., Araújo, A. C., Borma, L. S., Freitas, H. C., Goulden, M. L., Manzi, A. O., Miller, S. D., Nobre, A. D., Restrepo-Coupe, N., Saleska, S. R., Stöckli, R., von Randow, C., and Wofsy, S. C.: Surface ecophysiological behavior across vegetation and moisture gradients in tropical South America, Agr. Forest Meteorol., 182–183, 177–188, 2013.

Baldocchi, D. D. and Ma, S.: How will land use affect air temperature in the surface boundary layer? Lessons learned from a comparative study on the energy balance of an oak savanna and annual grassland in California, USA, Tellus B, 65, 19994, doi:10.3402/tellusb.v65i0.19994, 2013.

Baldocchi, D. D., Wilson, K., and Gu, L.: How the environment, canopy structure and canopy physiological functioning influence carbon, water and energy fluxes of a temperate broad-leaved deciduous forest-An assessment with the biophysical model CANOAK, Tree Phys., 22, 1065, 2002.

Ball, J. T., Woodrow, I. E., and Berry, J. A.: A model predicting stomatal conductance and its contribution to the control of photosynthesis under different environmental conditions, in: Progress in Photosynthesis Research, edited by: Biggins, J. and Nijhoff, M., Dordrecht, Martinus–Nijhoff Publishers, Dordrecht, the Netherlands, 5.221–5.224, 1987.

Blyth, E., Gash, J., Lloyd, A., Pryor, M., Weedon, G. P., and Shuttleworth, W. J.: Evaluating the JULES Land Surface Model Energy Fluxes Using FLUXNET Data, J. Hydrometeorol., 11, 509–519, doi:10.1175/2009JHM1183.1, 2010.

Boegh, E. and Soegaard, H.: Remote sensing based estimation of evapotranspiration rates, Int. J. Remote Sens., 25, 2535–2551, 2004.

Boegh, E., Soegaard, H., and Thomsen, A.: Evaluating evapotranspiration rates and surface conditions using Landsat TM to estimate atmospheric resistance and surface resistance, Remote Sens. Environ., 79, 329–343, 2002.

Bonan, G. B., Williams, M., Fisher, R. A., and Oleson, K. W.: Modeling stomatal conductance in the earth system: linking leaf water-use efficiency and water transport along the soil–plant–atmosphere continuum, Geosci. Model Dev., 7, 2193–2222, doi:10.5194/gmd-7-2193-2014, 2014.

Bosveld, F. C. and Bouten, W.: Evaluating a model of evaporation and transpiration with observations in a partially wet Douglas-fir forest, Bound.-Lay. Meteorol., 108, 365–396, 2003.

Boulet, G., Mougenot, B., Lhomme, J.-P., Fanise, P., Lili-Chabaane, Z., Olioso, A., Bahir, M., Rivalland, V., Jarlan, L., Merlin, O., Coudert, B., Er-Raki, S., and Lagouarde, J.-P.: The SPARSE model for the prediction of water stress and evapotranspiration components from thermal infra-red data and its evaluation over irrigated and rainfed wheat, Hydrol. Earth Syst. Sci., 19, 4653–4672, doi:10.5194/hess-19-4653-2015, 2015.

Bowen, I. S.: The ratio of heat losses by conduction and by evaporation from any water surface, Phys. Rev., 27, 779–787, 1926.

Brutsaert, W. and Stricker, H.: An advection-aridity approach to estimate actual regional evapotranspiration, Water Resour. Res., 15, 443– 450, 1979.

Chen, F. and Schwerdtfeger, P.: Flux-gradient relationships for momentum and heat over a rough natural surface, Q. J. Roy. Meteorol. Soc., 115, 335–352, 1989.

Chen, L., Zhang, Z., Li, Z., Tang, J., Caldwell, P., and Zhang, W.: Biophysical control of whole tree transpiration under an urban environment in Northern China, J. Hydrol., 402, 388–400, 2011.

Choudhury, B. J. and Monteith, J. L.: Implications of stomatal response to saturation deficit for the heat balance of vegetation, Agr. Forest Meteorol., 36, 215–225, 1986.

Christoffersena, B. O., Restrepo-Coup, N., Arain, M. A., Baker, I. T., Cestaro, B. P., Ciais, P., Fisher, J. B., Galbraith, D., Guan, X., Gulden, L., van den Hurk, B., Ichii, K., Imbuzeiro, H., Jain, A., Levine, N., Miguez-Macho, G., Poulter, B., Roberti, D. R., Sakaguchi, K., Sahoo, A., Schaefer, K., Shi, M., Verbeeck, H.,

Yang, Z. -L., Araújox, A. C., Kruijt, B., and Manzi, A. O.: Mechanisms of water supply and vegetation demand govern the seasonality and magnitude of evapotranspiration in Amazonia and Cerrado, Agr. Forest Meteorol., 191, 33–50, 2014.

Colaizzi, P. D., Kustas, W. P., Anderson, M. C., Agam, N., Tolk, J. A., Evett, S. R., Howell, T. A., Gowda, P. H., and O'Shaughnessya, S. A.: Two-source energy balance model estimates of evapotranspiration using component and composite surface temperatures, Adv. Water Resour., 50, 134–151, 2012.

Contini, D., Donateo, A., and Belosi, F.: Accuracy of Measurements of Turbulent Phenomena in the Surface Layer with an Ultrasonic Anemometer, J. Atmos. Ocean. Tech., 23, 785–801, doi:10.1175/JTECH1881.1, 2006.

Costa, M. H., Biajoli, M. C., Sanches, L., Malhado, A. C. M., Hutyra, L. R., da Rocha, H. R., Aguiar, R. G., and de Araújo, A. C.: Atmospheric versus vegetation controls of Amazonian tropical rain forest evapotranspiration: Are the wet and seasonally dry rain forests any different?, J. Geophys. Res., 115, G04021, doi:10.1029/2009JG001179, 2010.

Cox, P. M., Betts, R. A., Jones, C. D., Spall, S. A., and Totterdell, I. J.: Acceleration of global warming due to carbon-cycle feedbacks in a coupled climate model, Nature, 408, 184–187, 2000.

da Rocha, H. R., Goulden, M., Miller, S., Menton, M., Pinto, L., Freitas, H., and Figueira, A. S.: Seasonality of water and heat fluxes over a tropical forest in eastern Amazonia, Ecol. Appl., 14, 22–32, 2004.

da Rocha, H. R., Manzi, A. O., Cabral, O. M., Miller, S. D., Goulden, M. L., Saleska, S. R., Retro-Coupe, N., Wofsy, S. C., Borma, L. S., Artaxo, P., Vourlitis, G., Nogueira, J. S., Cardoso, F. L., Nobre, A. D., Kruijt, B., Freitas, H. C., von Randow, C., Aguiar, R. G., and Maia, J. F.: Patterns of water and heat flux across a biome gradient from tropical forest to savanna in Brazil, J. Geophys. Res., 114, G00B12, doi:10.1029/2007JG000640, 2009.

Davidson, E. A., de Araújo, A. C., Artaxo, P., Balch, J. K., Brown, I. F., Bustamante, M. M. C., Coe, M. T., DeFries, R. S., Keller, M., Longo, M., Munger, J. W., Schroeder, W., Soares-Filho, B. S., Souza, C. M., and Wofsy, S. C.: The Amazon basin in transition, Nature, 481, 321–328, 2012.

de Goncalves, L. G. G., Borak, J. S., Costa, M. H., Saleska, S. R., Baker, I., Restrepo-Coupe, N., Muza, M. N., Poulter, B., Verbeeck, H., Fisher, J. B., Arain, M. A., Arkin, P., Cestaro, B. P., Christoffersen, B., Galbraith, D., Guan, X., van den Hurk, B. J. J. M., Ichii, K., Imbuzeiro, H. M. A., Jain, A. K., Levine, N., Lu, C., Miguez-Macho, G., Roberti, D. R., Sahoo, A., Sakaguchi, K., Schaefer, K., Shi, M., Shuttleworth, W. J., Tian, H., Yang, Z.-L., and Zeng, X. : Overview of the Large-Scale Biosphere–Atmosphere Experiment in Amazonia Data Model Intercomparison Project (LBA-DMIP), Agr. Forest Meteorol., 182–183, 111–127, 2013.

Denmead, O. T. and Shaw, R. H.: Availability of soil water to plants as affected by soil moisture content and meteorological conditions, Agron. J., 54, 385–390, 1962.

Dolman, A. J., Miralles, D. G., and de Jeu, R. A. M.: Fifty years since Monteith's 1965 seminal paper: the emergence of global ecohydrology, Ecohydrology, 7, 897–902, doi:10.1002/eco.1505, 2014.

Drewry, D. T., Kumar, P., Long, S., Bernacchi, C., Liang, X. Z., and Sivapalan, M.: Ecohydrological responses of dense canopies to environmental variability: 1. Interplay between vertical structure and photosynthetic pathway, J. Geophys. Res.-Biogeo., 115, G04022, doi:10.1029/2010JG001340, 2010.

Ershadi, A., McCabe, M. F., Evans, J. P., and Wood, E. F.: Impact of model structure and parameterization on Penman–Monteith type evaporation models, J. Hydrol., 525, 521–535, 2015.

Farquhar, G. D.: Feedforward responses of stomata to humidity, Aust. J. Plant Physiol., 5, 787-800, 1978.

Foken, T.: 50 years of the Monin–Obukhov similarity theory, Bound.-Lay. Meteorol., 2, 7–29, 2006.

Gatti, L. V., Gloor, M., Miller, J. B., Doughty, C. E., Malhi, Y., Domingues, L. G., Basso, L. S., Martinewski, A., Correia, C. S. C., Borges, V. F., Freitas, S., Braz, R., Anderson, L. O., Rocha, H., Grace, J., Phillips, O. L., and Lloyd, J.: Drought sensitivity of Amazonian carbon balance revealed by atmospheric measurements, Nature, 506, 76–80, doi:10.1038/nature12957, 2014.

Gibson, L. A., Münch, Z., and Engelbrecht, J.: Particular uncertainties encountered in using a pre-packaged SEBS model to derive evapotranspiration in a heterogeneous study area in South Africa, Hydrol. Earth Syst. Sci., 15, 295–310, doi:10.5194/hess-15-295-2011, 2011.

Gloor, M., Brienen, R. J. W., Galbraith, D., Feldpausch, T. R., Schöngart, J., Guyot, J.-L., Espinoza, J. C., Lloyd, J., and Phillips, O. L.: Intensification of the Amazon hydrological cycle over the last two decades, Geophys. Res. Lett., 40, 1729–1733, 2013.

Harper, A., Baker, I. T., Denning, A. S., Randall, D. A., Dazlich, D., and Branson, M.: Impact of evapotranspiration on dry season climate in the Amazon Forest, J. Climate, 27, 574–591, doi:10.1175/JCLI-D-13-00074.1, 2014.

Hasler, N. and Avissar, R.: What controls evapotranspiration in the Amazon Basin, J. Hydrometeorol., 8, 380–395, doi:10.1175/JHM587.1, 2007.

Hilker, T., Lyapustin, A. I., Tucker, C. J., Hall, F. G., Myneni, R. B., Wang, Y., Bi, J., de Moura, Y. M., and Sellers, P. J.: Vegetation dynamics and rainfall sensitivity of the Amazon, P. Natl. Acad. Sci. USA, 111, 16041–16046, doi:10.1073/pnas.1404870111, 2014.

Holwerda, F., Bruijnzeela, L. A., Scatenac, F. N., Vugtsa, H. F., and Meestersa, A. G. C. A.: Wet canopy evaporation from a Puerto Rican lower montane rain forest: the importance of realistically estimated aerodynamic conductance, J. Hydrol., 414–415, 1–15, 2012.

Huntingford, C., Fisher, R. A., Mercado, L., Booth, B. B., Sitch, S., Harris, P. P., Cox, P. M., Jones, C. D., Betts, R. A., Malhi, Y., Harris, G. R., Collins, M., and Moorcroft, P.: Towards quantifying uncertainty in predictions of Amazon 'dieback', Philos. T. Roy. Soc. Lond. B, 363, 1857–1864, 2008.

Jarvis, P. G.: The interpretation of leaf water potential and stomatal conductance found in canopies in the field, Philos. T. Roy. Soc. Lond. B, 273, 593–610, 1976.

Jarvis, P. G.: Transpiration and assimilation of trees and agricultural crops: the 'omega' factor, in: Attributes of Trees and Crop Plants, edited by: Cannell, M. G. R. and Jackson, J. E., Institute of terrestrial Ecology, Edinburg, UK, 460–480, 1986.

Jarvis, P. G. and McNaughton, K. G.: Stomatal control of transpiration: scaling up from leaf to region, Adv. Ecol. Res., 15, 1–49, 1986.

Jones, H. G.: Stomatal control of photosynthesis and transpiration, J. Exp. Bot., 49, 387–398, 1998.

Kumagai, T., Saitoh, T. M., Sato, Y., Morooka, T., Manfroi, O. J., Kuraji, K., and Suzuki, M.: Transpiration, canopy conductance and the decoupling coefficient of a lowland mixed dipterocarp forest in Sarawak, Borneo: dry spell effects, J. Hydrol., 287, 237–251, 2004.

Kustas, W. P. and Anderson, M. C.: Advances in thermal infrared remote sensing for land surface modeling, Agr. Forest Meteorol., 149, 2071–2081, 2009.

Lawrence, D. and Vandecar, K.: Effects of tropical deforestation on climate and agriculture, Nat. Clim. Change, 5, 27–36, doi:10.1038/nclimate2430, 2015.

Leuning, R.: A critical appraisal of a combined stomatal – photosynthesis model for C3 plants, Plant Cell Environ., 18, 339–355, 1995.

Leuzinger, S. and Kirner, C.: Rainfall distribution is the main driver of runoff under future CO_2-concentration in a temperate deciduous forest, Global Change Biol., 16, 246–254, 2010.

Lhomme, J. P. and Montes, C.: Generalized combination equations for canopy evaporation under dry and wet conditions, Hydrol. Earth Syst. Sci., 18, 1137–1149, doi:10.5194/hess-18-1137-2014, 2014.

Loescher, H. W., Gholz, H. L., Jacobs, J. M., and Oberbauer, S. F.: Energy dynamics and modeled evapotranspiration from a wet tropical forest in Costa Rica, J. Hydrol., 315, 274–294, 2005.

Ma, N., Zhang, Y., Guo, Y., Gao, H., Zhang, H., and Wang, Y.: Environmental and biophysical controls on the evapotranspiration over the highest alpine steppe, J. Hydrol., 529, 980–992, 2015.

Malhi, Y.: The productivity, metabolism and carbon cycle of tropical forest vegetation, J. Ecol., 100, 65–75, 2012.

Malhi, Y., Pegoraro, E., Nobre, A. D., Pereira, M. G. P., Grace, J., Culf, A. D., and Clement, R.: The energy and water dynamics of a central Amazonian rain forest, J. Geophys. Res., 107, 8061, doi:10.1029/2001JD000623, 2002.

Mallick, K., Jarvis, A. J., Boegh, E., Fisher, J. B., Drewry, D. T., Tu, K. P., Hook, S. J., Hulley, G., Ardö, J., Beringer, J., Arain, A., and Niyogi, D.: A surface temperature initiated closure (STIC) for surface energy balance fluxes, Remote Sens. Environ., 141, 243–261, 2014.

Mallick, K., Boegh, E., Trebs, I., Alfieri, J. G., Kustas, W. P., Prueger, J. H., Niyogi, D., Das, N., Drewry, D. T., Hoffmann, L., and Jarvis, A. J.: Reintroducing radiometric surface temperature into the Penman–Monteith formulation, Water Resour. Res., 51, 6214–6243, doi:10.1002/2014WR016106, 2015.

Massman, W. J.: A model study of kB_H^{-1} for vegetated surfaces using 'localized near-field' Lagrangian theory, J. Hydrol., 223, 27–43, 1999.

Matheny, A. M., Bohrer, G., Stoy, P., Baker, I. T., Black, A. T., Desai, A. R., Dietze, M. C., Gough, C. M., Ivanov, V. Y., Jassal, R. S., Novick, K. A., Schäfer, K. V. R., and Verbeeck, H.: Characterizing the diurnal patterns of errors in the prediction of evapotranspiration by several land-surface models: An NACP analysis, J. Geophys. Res.-Biogeo., 119, 1458–1473, doi:10.1002/2014JG002623, 2014.

Matzner, S. and Comstock, J.: The temperature dependence of shoot hydraulic resistance: implications for stomatal behaviour and hydraulic limitation, Plant Cell Environ., 24, 1299–1307, 2001.

McNaughton, K. G. and Jarvis, P. G.: Using the Penman–Monteith equation predictively, Agr. Water Manage., 8, 263–278, 1984.

McNaughton, K. G. and Jarvis, P. G.: Effects of spatial scale on stomatal control of transpiration, Agr. Forest Meteorol., 54, 279–301, 1991.

Medlyn, B. E., Duursma, R. A., Eamus, D., Ellsworth, D. S., Prentice, I. C., Bartons, C. V. M., Crous, K. Y., de Angelis, P., Freeman, M., and Wingate, L.: Reconciling the optimal and empirical approaches to modelling stomatal conductance, Global Change Biol., 17, 2134–2144, doi:10.1111/j.1365-2486.2010.02375.x, 2011.

Meinzer, F. C., Goldstein, G., Holbrook, N. M., Jackson, P., and Cavelier, J.: Stomatal and environmental control of transpiration in a lowland tropical forest site, Plant Cell Environ., 16, 429–436, 1993.

Meinzer, F. C., Andrade, J. L., Goldstein, G., Holbrook, N. M., Cavelier, J., and Jackson, P.: Control of transpiration from upper canopy of a tropical forest: the role of stomatal, boundary layer and hydraulic architecture components, Plant Cell Environ., 20, 1242–1252, 1997.

Mercado, L. M., Lloyd, J., Dolman, A. J., Sitch, S., and Pati, S.: Modelling basin-wide variations in Amazon forest productivity – Part 1: Model calibration, evaluation and upscaling functions for canopy photosynthesis, Biogeosciences, 6, 1247–1272, doi:10.5194/bg-6-1247-2009, 2009.

Miglietta, F., Peressotti, A., Viola, R., Körner, C., and Amthor, J. S.: Stomatal numbers, leaf and canopy conductance, and the control of transpiration, P. Natl. Acad. Sci. USA, 108, E275–E275, 2011.

Monteith, J. L.: Evaporation and environment, in: Symposium of the Society for Experimental Biology, The State and Movement of Water in Living Organisms, edited by: Fogg, G. E., Academic Press, Inc., NY, 205–234, 1965.

Monteith, J. L.: Evaporation and surface temperature, Q. J. Roy. Meteorol. Soc., 107, 1–27, 1981.

Monteith, J. L.: Accommodation between transpiring vegetation and the convective boundary layer, J. Hydrol., 166, 251–263, 1995.

Monteith, J. L. and Unsworth, M. H.: Principles of Environmental Physics, Elsevier, Amsterdam, 2008.

Motzer, T., Munz, N., Kuppers, M., Schmitt, D., and Anhuf, D.: Stomatal conductance, transpiration and sap flow of tropical montane rain forest trees in the southern Ecuadorian Andes, Tree Physiol., 25, 1283–1293, 2005.

Ocheltree, T. W., Nippert, J. B., and Prasad, P. V. V.: Stomatal responses to changes in vapor pressure deficit reflect tissue-specific differences in hydraulic conductance, Plant Cell Environ., 37, 132–139, 2014.

O'Grady, A. P., Eamus, D., and Hutley, L. B.: Transpiration increases during the dry season: patterns of tree water use in eucalypt open-forests of northern Australia, Tree Physiol., 19, 591—597, 1999.

Penman, H. L.: Natural evaporation from open water, bare soil, and grass, P. Roy. Soc. Lond. A, 193, 120–146, 1948.

Priante-Filho, N., Vourlitis, G. L., Hayashi, M. M. S., De Souza Nogueira, J., Campelo Jr., J. H., Nunes, P. C., E Souza, L. S., Couto, E. G., Hoeger, W., Raiter, F., Trienweiler, J. L., Miranda, E. J., Priante, P. C., Fritzen, C. L., Lacerda, M., Pereira, L. C., Biudes, M. S., Suli, G. S., Shiraiwa, S., Do Paulo, S. R., and Silveira, M.: Comparison of the mass and energy exchange of a

pasture and a mature transitional tropical forest of the southern Amazon Basin during a seasonal transition, Global Change Biol., 10, 863–876, doi:10.1111/j.1529-8817.2003.00775.x, 2004.

Priestley, C. H. B. and Taylor, R. J.: On the assessment of surface heat flux and evaporation using large scale parameters, Mon. Weather Rev., 100, 81–92, 1972.

Prihodko, L., Denning, A. S., Hanan, N. P., Baker, I. T., and Davis, K.: Sensitivity, uncertainty and time dependence of parameters in a complex land surface model, Agr. Forest Meteorol., 148, 268–287, 2008.

Raupach, M. R.: Vegetation-atmosphere interaction and surface conductance at leaf, canopy and regional scales, Agr. Forest Meteorol., 73, 151-179, 1995.

Raupach, M. R.: Influence of local feedbacks on land-air exchanges of energy and carbon, Global Change Biol., 4, 477–494, 1998.

Raupach, M. R. and Finnigan, J. J.: Scale issues in boundary-layer meteorology: surface energy balance in heterogeneous terrain, Hydrol. Process., 9, 589–612, 1995.

Renner, M., Hassler, S. K., Blume, T., Weiler, M., Hildebrandt, A., Guderle, M., Schymanski, S. J., and Kleidon, A.: Dominant controls of transpiration along a hillslope transect inferred from ecohydrological measurements and thermodynamic limits, Hydrol. Earth Syst. Sci., 20, 2063–2083, doi:10.5194/hess-20-2063-2016, 2016.

Restrepo-Coupe, N., da Rocha, H. R., Hutyra, L. R., da Araujo, A. C., Borma, L. S., Christoffersen, B., Cabral, O. M. R., de Camargo, P. B., Cardoso, F. L., da Costa, A. C. L., Fitzjarrald, D. R., Goulden, M. L., Kruijt, B., Maiai, J. M. F., Malhi, Y. S., Manzi, A. O., Miller, S. D., Nobre, A. D., von Randow, C., Ság, L. D. A., Sakai, R. K., Tota, J., Wofsy, S. C., and Zanchi, F. B.: What drives the seasonality of photosynthesis across the Amazon basin? A cross-site analysis of eddy flux tower measurements from the Brasil flux network, Agr. Forest Meteorol., 182–183, 128–144, 2013.

Richiardone, R., Manfrin, M., Ferrarese, S., Francone, C., Fernicola, V., Gavioso, R. M., and Mortarini, L.: Influence of the Sonic Anemometer Temperature Calibration on Turbulent Heat-Flux Measurements, Bound.-Lay. Meteorol., 142, 425–442, 2012.

Roy, S. B. and Avissar, R.: Impact of land use/land cover change on regional hydrometeorology in Amazonia, J. Geophys. Res., 107, 2156–2202, doi:10.1029/2000JD000266, 2002.

Saleska, S. R., da Rocha, H. R., Huete, A. R., Nobre, A. D., Artaxo, P., and Shimabukuro, Y. E.: LBA-ECO CD-32 Flux Tower Network Data Compilation, Brazilian Amazon: 1999–2006, Data set, available at: http://daac.ornl.gov from Oak Ridge National Laboratory Distributed Active Archive Center, Oak Ridge, Tennessee, USA, doi:10.3334/ORNLDAAC/1174, 2013.

Shuttleworth, W. J., Gurney, R. J., Hsu, A. Y., and Ormsby, J. P.: FIFE: The variation in energy partition at surface flux sites, in Remote Sensing and Large Scale Processes, in: Proceedings of the IAHS Third International Assembly, vol. 186, edited by: Rango, A., IAHS Publ., Baltimore, Md, 67–74, 1989.

Shuttleworth, W. J.: Micrometeorology of temperate and tropical forest, Philos. T. Roy. Soc. Lond. B, 324, 299–334, 1989.

Shuttleworth, W. J.: Putting the "vap" into evaporation. Hydrol. Earth Syst. Sci., 11, 210–244, doi:10.5194/hess-11-210-2007, 2007.

Shuttleworth, W. J. and Wallace, J. S.: Evaporation from sparse crops – an energy combination theory, Q. J. Roy. Meteorol. Soc., 111, 839–855, 1985.

Simpson, I. J., Thurtell, G. W., Nuemann, H. H., den Hartog, G., and Edwards, G. C.: The validity of similarity theory in the roughness sublayer above forests, Bound.-Lay. Meteorol., 87, 69–99, 1998.

Stella, P., Kortner, M., Ammann, C., Foken, T., Meixner, F. X., and Trebs, I.: Measurements of nitrogen oxides and ozone fluxes by eddy covariance at a meadow: evidence for an internal leaf resistance to NO_2, Biogeosciences, 10, 5997–6017, doi:10.5194/bg-10-5997-2013, 2013.

Streck, N. A.: Stomatal response to water vapor pressure deficit: an unsolved issue, Revista Brasil, Agrociên, 9, 317–322, 2003.

Thom, A. S., Stewart, J. B., Oliver, H. R., and Gash, J. H. C.: Comparison of aerodynamic and energy budget estimates of fluxes over a pine forest, Q. J. Roy. Meteorol. Soc., 101, 93–105, 1975.

Tuzet, A., Perrier, A., and Leuning, R.: A coupled model of stomatal conductance, photosynthesis and transpiration, Plant Cell Environ., 26, 1097–1116, 2003.

van der Tol, C., van der Tol, S., Verhoef, A., Su, B., Timmermans, J., Houldcroft, C., and Gieske, A.: A Bayesian approach to estimate sensible and latent heat over vegetated land surface, Hydrol. Earth Syst. Sci., 13, 749–758, doi:10.5194/hess-13-749-2009, 2009.

van Dijk, A. I. J. M., Gash, J. H., van Gorsel, E., Blanken, P. D., Cescatti, A., Emmel, C., Gieleng, B., Harman, I. N., Kiely, G., Merbold, L., Montagnani, L., Moors, E., Sottocornola, M., Varlagin, A., Williams, C. A., and Wohlfahrt, G.: : Rainfall interception and the couple surface water and energy balance, Agr. Forest Meteorol., 214–215, 402–415, 2015.

Venturini, V., Islam, S., and Rodriguez, L.: Estimation of evaporative fraction and evapotranspiration from MODIS products using a complementary based model, Remote Sens. Environ., 112, 132–141, 2008.

Villagarcía, L., Were, A., García, M., and Domingo, F.: Sensitivity of a clumped model of evapotranspiration to surface resistance parameterisations: Application in a semi-arid environment, Agr. Forest Meteorol., 150, 1065–1078, 2010.

Villani, M. G., Schmid, H. P., Su, H. B., Hutton, J. L., and Vogel, C. S.: Turbulence statistics measurements in a northern hardwood forest, Bound.-Lay. Meteorol., 108, 343–364, 2003.

von Randow, R. C. S., von Randow, C., Hutjes, R. W. A., Tomasella, J., and Kruijt, B.: Evapotranspiration of deforested areas in central and southwestern Amazonia, Theor. Appl. Climatol., 109, 205–220, doi:10.1007/s00704-011-0570-1, 2012.

Zhang, Q., Manzoni, S., Katul, G., Porporato, A., and Yang, D.: The hysteretic evapotranspiration-vapor pressure deficit relation, J. Geophys. Res.-Biogeo., 119, 125–140, doi:10.1002/2013JG002484, 2014.

Zuecco, G., Penna, D., Borga, M., and van Meerveld, H. J.: A versatile index to characterize hysteresis between hydrological variables at the runoff event timescale, Hydrol. Process., 30, 1449–1466, doi:10.1002/hyp.10681, 2016.